Universidade de Aveiro
Ano 2018

Departamento de Química

JOÃO PEDRO FERNANDES CARVALHO

Nanossistemas multicamada para a libertação controlada de fármacos anticancerígenos

Multi-layered nanosystems for the controlled release of anticancer drugs

Universidade de Aveiro
Ano 2018

Departamento de Química

JOÃO PEDRO FERNANDES CARVALHO

Nanossistemas multicamada para a libertação controlada de fármacos anticancerígenos

Multi-layered nanosystems for the controlled release of anticancer drugs

Dissertação apresentada à Universidade de Aveiro para cumprimento dos requisitos necessários à obtenção do grau de Mestre em Bioquímica – Ramo de Bioquímica Clínica, realizada sob a orientação científica da Doutora Carmen Sofia da Rocha Freire Barros, Investigadora Principal do CICECO – Instituto de Materiais de Aveiro, Universidade de Aveiro e da Doutora Carla Andreia Cunha Vilela, Investigadora de Pós-Doutoramento do CICECO – Instituto de Materiais de Aveiro, Universidade de Aveiro

o júri

presidente

Professor Doutor Brian James Goodfellow
Professor Auxiliar da Universidade de Aveiro

Doutora Helena Cristina Correia de Oliveira
Bolseira de Pós-Doutoramento da Universidade de Aveiro

Doutora Carmen Sofia da Rocha Freire Barros
Investigadora Principal do CICECO – Instituto de Materiais de Aveiro da Universidade de Aveiro

agradecimentos

O primeiro agradecimento que gostaria de deixar expresso é para com as minhas orientadoras neste projeto, a Dr.ª Carla Vilela e a Dr.ª Carmen Freire. Sem a sua orientação dedicada, disponibilidade total e admirável paciência, tudo teria sido indubitavelmente mais difícil.

Nesse sentido, o agradecimento seguinte vai para o Dr. Ricardo Pinto por todos os ensinamentos, toda a ajuda e pela motivação e amizade, não só durante a síntese, mas ao longo de todo este trabalho. Agradeço também ao Tiago Carvalho e ao Nuno Silva a preciosa ajuda em tudo o que às nanofibrilas de lisozima diz respeito. Ao João Barbosa, à Verónica Bastos e à Dr.ª Helena agradeço todo o acompanhamento nos ensaios biológicos deste trabalho.

Um especial agradecimento à Ana Miguel, companheira nesta jornada, pelos ensinamentos, pelo apoio e pela boa disposição. A ela e à Adriana Pais um sentido obrigado pela amizade e por todos os bons momentos no laboratório.

Agradeço também à Bárbara Sousa e ao Pedro Corda, amigos incansáveis em todas as horas, que fazem de Aveiro uma casa para mim todos os dias. Sem eles, e sem os sorrisos que me trazem sempre, os meus dias seriam bem mais escuros.

Ao Carlos, à Helena, à Margarida e ao Zé um especial obrigado pela amizade, pela música, pela animação e pela paciência ao longo destes meses. À Diana e à Beatriz, obrigado por encurtarem os quilómetros e me aquecerem sempre o coração com as palavras certas. À prof. Isabel e ao prof. Hélder, obrigado pela música, por todo o apoio e pela compreensão ao longo desta etapa.

Um obrigado sincero aos meus pais, Palmira e Firmino, por todas as oportunidades que me proporcionam e por nunca deixarem de acreditar em mim e no meu potencial. São a razão de ser quem sou. À minha irmã Rita, um obrigado do tamanho do mundo pelo amor incondicional e pela amizade e companheirismo que nos unirão para sempre.

Por fim, mas não menos importante, obrigado a toda a minha família e amigos, que mesmo quando estão longe são o meu apoio e a razão para que eu seja feliz, todos os dias.

palavras-chave

Sistemas multicamada, montagem camada-a-camada, nanopartículas, nanotransportadores, biopolímeros, quitosano, alginato, libertação controlada, fármacos anticancerígenos, curcumina, nanofibrilas de lisozima.

resumo

O cancro é uma das principais causas de morte no mundo, e as opções terapêuticas atuais apresentam inúmeros inconvenientes. A quimioterapia, especificamente, possui efeitos secundários reconhecidos. No entanto, e graças ao desenvolvimento tecnológico e científico dos últimos anos, surge na nanomedicina uma nova abordagem para este dilema: a utilização de nanossistemas capazes de libertar fármacos anticancerígenos de forma controlada e apenas em células designadas. Estes nanossistemas podem ser obtidos a partir de inúmeros materiais, incluindo biopolímeros, e por variadas técnicas.

Neste contexto, o trabalho desenvolvido nesta dissertação consiste na síntese e caracterização de nanopartículas obtidas por montagem camada-a-camada a partir de *templates* esféricos de SiO_2 amino-modificados (diâmetro: 234 ± 19 nm). A deposição alternada de biopolímeros – alginato (ALG) e quitosano (CH) ou nanofibrilas de lisozima (LNFs) - em *templates* com curcumina previamente incorporada deu origem a nanopartículas cobertas por ALG/CH (com 243 ± 8 nm de diâmetro) ou por ALG/LNFs (com 242 ± 8 nm). A sistemática reversão do potencial-zeta e a observação das partículas por microscopia eletrónica de varrimento (SEM) confirma a deposição de cada camada de biopolímero.

O presente trabalho inclui também a avaliação do perfil de libertação do fármaco a partir destas nanopartículas multicamada, demonstrando-se uma libertação mais controlada do que em partículas sem camadas de biopolímeros. A avaliação da capacidade citotóxica em células humanas de cancro do fígado (HepG2) foi posteriormente avaliada através de um ensaio com MTT. O efeito citotóxico das partículas contendo CUR e cobertas de polímeros revelou-se semelhante ao das partículas análogas sem camadas, demonstrando que as duas camadas de biopolímeros (ALG/CH ou ALG/LNFs) não comprometem o potencial citotóxico das mesmas.

keywords

Multi-layered systems, layer-by-layer assembly, nanoparticles, nanocarriers, biopolymers, chitosan, alginate, controlled release, anticancer drugs, curcumin, lysozyme nanofibrils.

abstract

Cancer is one of the leading causes of death worldwide, and current therapeutic options present numerous drawbacks. Chemotherapy, specifically, is associated with widely known side effects. However, and due to the scientific and technologic advances of the past years, a new approach to this dilemma appears in nanomedicine: the use of nanosystems capable of releasing the anticancer drugs in a controlled way and only at the designated cells. These nanosystems may be obtained from numerous materials, including biopolymers, and by various techniques.

Specifically, the work described here consists in the synthesis and characterization of nanoparticles obtained by layer-by-layer assembly from amino-modified spherical SiO_2 templates (diameter: 234 ± 19 nm). The alternate deposition of biopolymers - alginate (ALG) and chitosan (CH) or lysozyme nanofibrils (LNFs) - on templates pre-loaded with curcumin allowed the creation of nanoparticles covered in ALG/CH (with a diameter of 243 ± 8 nm) or ALG/LNFs (with 242 ± 8 nm). The systematic reversion the zeta-potential and the observation of the particles by scanning electron microscopy (SEM) confirms the deposition of each biopolymeric layer.

The present work also includes the evaluation of the release profile of this drug from the multi-layered nanoparticles, demonstrating a more controlled release than with the bare counterparts. The evaluation of their cytotoxic capacity in human liver cancer cell line (HepG2) was posteriorly evaluated through an MTT assay. The cytotoxic effect of layered particles containing CUR was similar to the unlayered counterparts', demonstrating that the two layers of biopolymers (ALG/CH or ALG/LNFs) do not compromise their cytotoxic potential.

Abbreviations

ALG	Alginate
APP	(4-amino-2-(2-hydroxy-1-decyl)pyrazole-[3,4-d]pyrimidine)
APTES	(3-aminopropyl)triethoxysilane
BSA	Bovine-serum albumin
CH	Chitosan
CUR	Curcumin
DES	Deep eutectic solvent
DMEM	Dulbecco's modified eagle medium
DMSO	Dimethyl sulfoxide
DNA	Deoxyribonucleic acid
DOX	Doxorubicin
EGFR	Epidermal growth factor receptor
FBS	Fetal bovine serum
FITC	Fluorescein isothiocyanate
HA	Hyaluronic acid
HEC-1A	Human endometrial adenocarcinoma cells
HEWL	Hen egg white lysozyme
HSA	Human-serum albumin
huA33mAb	Humanized A33 monoclonal antibody
LbL assembly	Layer-by-layer assembly
LNFs	Lysozyme nanofibrils
MTT	3-(4,5-Dimethylthiazolyl-2)-2,5-diphenyltetrazolium bromide
NCHS	National Centre for Health Statistics
NCI–SEER	National Cancer Institute Surveillance, Epidemiology and End Results Program
NIR	Near-infrared
PAGs	Photoacid generators

PAH	Poly(allylamine hydrochloride)
PBS	Phosphate-buffered saline
PEG	Poly(ethylene glycol)
PLA	Poly(lactic acid)
PLGA	Poly(L-glutamic-acid)
PLL	Poly(L-lysine)
PMMA	Poly(methyl methacrylate)
PSS	Poly(styrene sulfonate)
PTX	Paclitaxel
RNA	Ribonucleic acid
SCC7	Squamous cell carcinoma cells
SEM	Scanning electron microscopy
STEM	Scanning transmission electron microscopy
TEOS	Tetraethoxysilane
UV-Vis	Ultraviolet–visible
WHO	World Health Organization

Contents

List of Figures

List of Tables

1 Introduction

1.1 Cancer: an overview

1.1.1 Epidemiology, incidence and survival rate

Cancer is one of the leading causes of death worldwide. The Word Health Organization (WHO) estimates that between 2010 and 2015, 8.8 million cancer deaths were registered, and the number of new cases is expected to rise by about 70% over the next two decades.[1,2] In the United States, the National Centre for Health Statistics (NCHS) and the National Cancer Institute Surveillance, Epidemiology and End Results Program (NCI – SEER) estimate that 1,735,350 people will be diagnosed with cancer in America in the current year of 2018 (which translates in about 4700 new cases per day) and 609,640 persons will die because of it (about 1700 deaths every day).[3] The impact of this social burden makes Oncology an area of increasing interest, and the research of new therapeutic approaches has led to an overall improvement of the panorama: over the last 30 years, the survival rate for all cancers has increased in over 20%.[4] By the first day of 2016, more than 15.5 million Americans with a history of cancer were still alive – but the projections say this number will increase to over 20 million in 2026.[5] Even so, nearly 22% of all the deaths on the US in 2015 were due to cancer, which makes it the second leading cause of death in this region, being surpassed only by heart diseases.[3]

In Europe, WHO estimates around 3,7 million new cases and 1,9 million deaths each year, making this the second most common cause of death, similarly to what is described for the US. Specifically in Portugal, WHO described a total of 27,200 deaths attributed to cancer in 2014, which translates to more than 28% of the total number of deaths for this region.[6]

1.1.2 General pathophysiology of cancer

Even though defining cancer might not be an easy task, one is able to specify the most recognizable trait of this disease: the uncontrolled proliferation of mutated cells and invasion of healthy tissues.[7] Healthy ("normal") cells usually multiply through a process called mitosis. This complex process is highly controlled at multiple checkpoints during the cell cycle to avoid the proliferation of cells with significant structural deviations and defects on their DNA. Cells with detected abnormalities have their lifecycle arrested and then begin a process of programmed cell suicide – apoptosis. Cancer cells are generally a product of DNA mutations that allow them to circumvent the mitotic control (and apoptosis) and to replicate exponentially, invading nearby tissues and creating an irregular agglomerate of mutated cells – a tumour (Figure 1).[8]

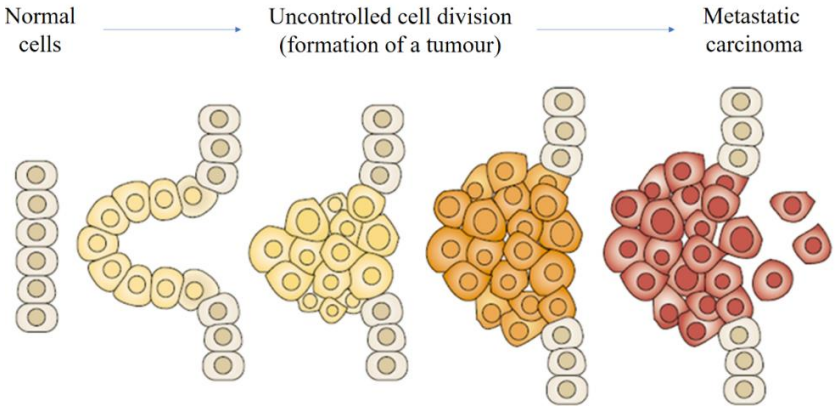

Figure 1 - Formation of a tumour. Adapted from "Two genetic hits (more or less) to cancer" Knudson (2001)[9]

Between the most significant DNA abnormalities correlated with cancer, mutations at proto-oncogenes and tumour-suppressor genes are some of the most widely described. Proto-oncogenes are DNA sequences involved in the stimulation of cell growth and division. Mutations that result in an over-expression of such genes or in any way that amplify their effect can result in the development of uncontrolled cellular replication. On the other hand, tumour-suppressor genes (like the well-known TP53[10]) are those involved in the checkpoint processes that arrest cell division when damages to DNA are present. Alterations to these

genes that reduce or refrain this control will allow mutated cells to replicate indefinitely and possibly result in the formation of a tumour.[11]

The search for cancer causes has led to the identification of multiple factors as sources of such mutations at these cells' genetic material. While some (like the exposure to ionizing radiation and hazardous chemicals) might occur accidentally during one's lifetime, there are some behavioural factors that have been shown to contribute to this scenario - specially tobacco smoking, alcohol consumption, obesity, low physical activity and even poor dietary habits.[12] However, the contribution of these habits to the development of neoplasms is quite complex, and the underlying mechanisms are still under intense investigation. Some infectious agents have also been described as potentially mutagenic factors, specially the hepatitis C and B virus, human papillomaviruses, and bacteria like *Helicobacter pylori*. Altogether, these four pathogens have been held responsible for more than 90% of the cancer cases related to infectious agents.[13]

Another rather important capability of cancer cells is the aptitude to stimulate the growth of new blood vessels nearby, so the flow of nutrients and oxygen is enough for the tumour to prosper – the so-called angiogenesis. This angiogenesis in the tumour is achieved by the release of certain growth factors - including the ones encompassed in the vascular endothelial growth factor family (VEGF) - by cells.[14] The resulting blood vessels are usually structurally and functionally abnormal, giving the tumours a chaotic architecture and irregular blood flow.[15]

Frequently, invasive cancer cells reach the circulatory vessels and migrate to different sites where they originate new tumours in a process called metastasis. Talmadge *et al.*[16] defines metastasis as the process involving the invasion of blood or lymphatic vessels by mutated cells, their transit through these systems, extravasation from circulation and setting at distant sites where they will form small nodules of microscopic size (micrometastasis) (Figure 2). The replication of mutated cells at these sites, and consequent growing of these micrometastasis, gives rise to macroscopic tumours. These tumours are autonomous from the original site, frequently developing different characteristics due to their own posterior mutations of the same genetic material.[16]

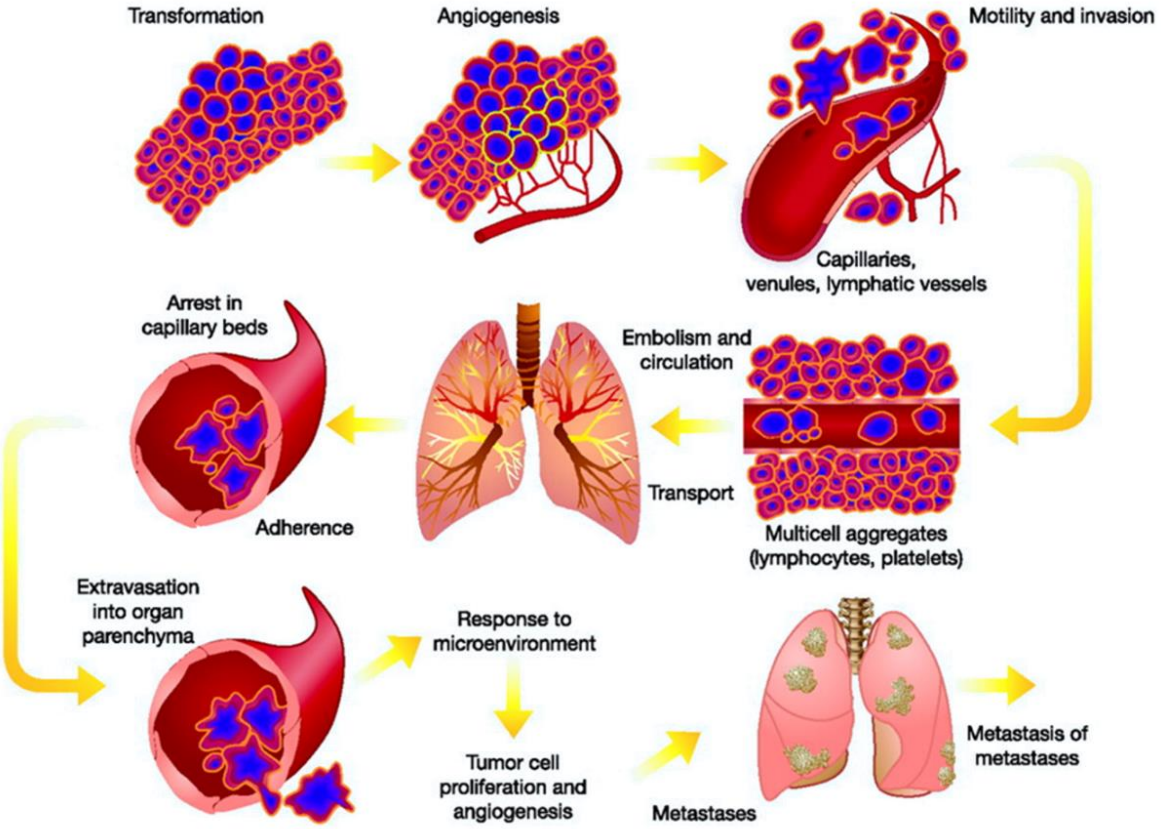

Figure 2 - The sequential process of metastasis. Reproduced from "The Biology of Cancer Metastasis: Historical Perspective" Talmadge et al. (2010)[16]

The characteristics described above are generally common to all types of cancer. Thus, Hanahan *et al*.[8] stablished the ten hallmark capabilities of cancer cells as: i) sustaining proliferative signalling; ii) evading growth suppressors; iii) avoiding immune destruction; iv) enabling replicative immortality; v) tumour-promoting inflammation; vi) activating invasion and metastasis; vii) inducing angiogenesis; viii) genome instability and mutation; ix) resisting cell death; and x) deregulating cellular energetics (Figure 3). Overall, this means that these cells can evade or resist every defence mechanism of the body, while maintaining a high proliferative rate and creating optimal conditions to thrive.

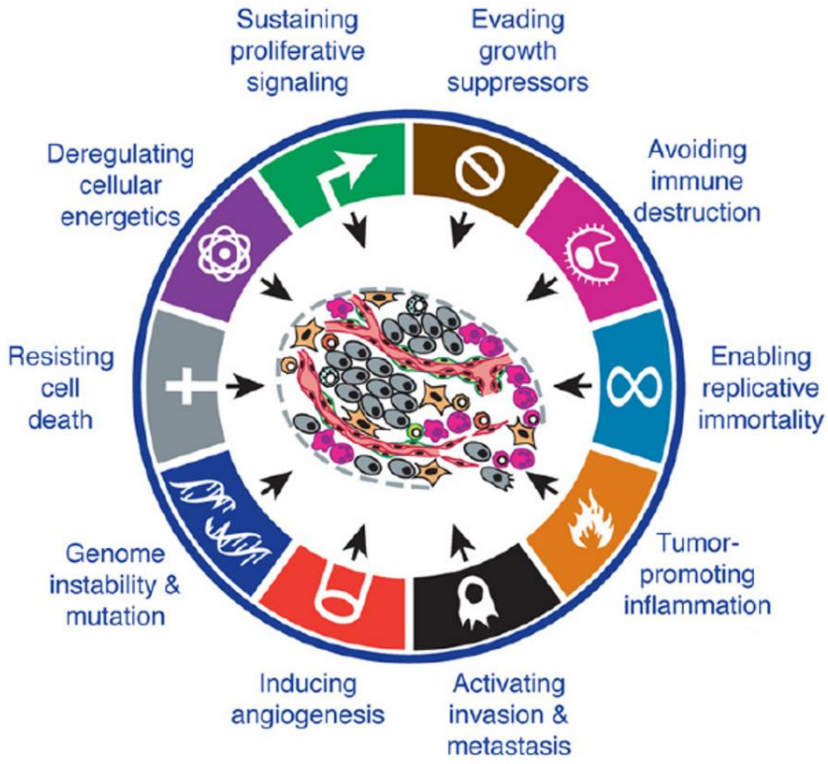

Figure 3 - The ten hallmarks of cancer cells as proposed by Hanahan et al. Adapted from "Hallmarks of Cancer: The next generation" (2011)[8]

1.1.3 Current treatment options

The treatment of oncologic diseases is an interplay of several techniques and principles, aiming the reduction/removal of the tumour and of the mutated cells from the organism (Figure 4). One of the main approaches after the diagnosis of cancer is the surgical removal of the tumour itself. Progresses in medical imaging techniques have allowed the precise determination of the extent and location of the tumour, leading to an increase of the success of tumour-removing surgeries.[17] Yet, the surgical removal of the unhealthy tissues is often disfiguring and does not grant the complete cure from cancer: even though the tumour is excised with a surrounding margin of healthy tissue, the existence of metastatic spread might mean a reoccurrence of oncologic disease in the future.

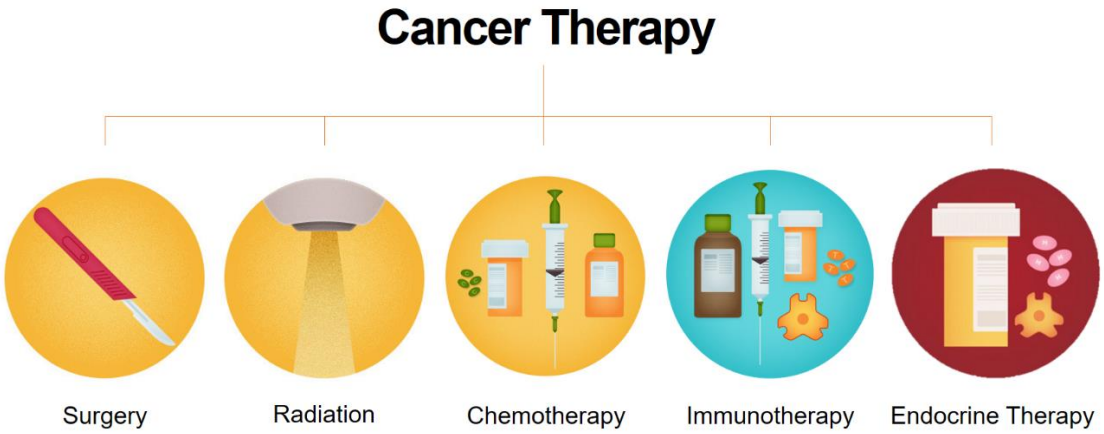

Figure 4 - Most common therapeutic approaches for cancer treatment. Adapted from National Breast Cancer Foundation, Inc website[18]

Radiation therapy is also widely used when treating cancer. It relies on the use of localized ionizing radiation (IR), such as gamma and X-rays, to destroy specific cells. IR has the capability to penetrate through tissues and affect the cells by causing severe genetic defects and inducing cell death.[19] However, radiation therapy is (just like surgery) a local procedure that is not enough to deal with metastasis, and even though it is able to reach regions of the body where surgery is not viable, its' damaging effects to the healthy tissues that surround the tumour can be quite extensive. Some cancer cells actually exhibit an extensive resistance to IR induced apoptosis.[20]

Regarding systemic procedures, immunotherapy, endocrine therapy and chemotherapy are the main options available for cancer patients. In immunotherapy, the immune system of the organism itself is stimulated to fight against malignant cells using cytokines, antibodies or modified immune cells.[21] This approach relies on the existence of cells from the immune system with the capacity to recognize and attack specific targets. These cells (specially T-cells and dendritic cells) are able to identify antigens which are either overexpressed or aberrant at cancer cells' surface, and initiate an immune response against them.[22] The high cost and complexity of this method, however, makes it an alternative that is not easily available for every patient.

Endocrine therapy relies on the modulation of hormone-dependent pathways of cancer cells. Certain types of cancer (like breast, prostate or endometrial cancer), originated from hormone-sensitive tissues, grow in response to hormones that stimulate cell proliferation. Therefore, one could be able to minimize the growth of such tumours by blocking the receptors for these hormones at cancer cells, or by reducing the endogenous hormone production. This is frequently achieved by administering drugs that compete against these hormones by binding to their receptors (like tamoxifen), or by the surgical removal of the hormone-producing organs.[23] However, not all tumours arising from hormone-sensitive tissues are affected by this approach, since the tumour cells themselves might become hormone-resistant, or the suppression of endogenous hormone production might be insufficient.[24]

Chemotherapy is still the standard for cancer treatment. It consists in the injection of a cytotoxic drug into the bloodstream, being therefore able to reach nearly every location in the body.[25] These cytotoxic drugs interfere with the mitotic process, inhibiting cell division and consequently arresting the tumour growth. Since these cytotoxic agents target fast-dividing cells, most cancer cells are usually extensively affected by such drugs, but so are healthy cells with a high replication rate - like hair follicles, bone marrow cells or even some of the cells in the digestive tract. This is one of the reasons why chemotherapy is often associated with severe side-effects like alopecia, nausea, vomiting, fatigue, and even with a depression of the immune system – immunosuppression.[26]

There are several types of drugs considered in chemotherapy regimens.[25] Alkylating agents (like cyclophosphamide) are commonly used, since they react with DNA, causing single and double-strand breaks that compromise cell survival. Antimetabolites (*e.g.* 5-fluoroacil) also affect DNA synthesis: since they closely resemble purines and pyrimidines, they get incorporated in DNA/RNA strands and cause breaks or premature chain termination. Anthracyclines (like doxorubicin) are antibiotics that can similarly intercalate with DNA, generating breaks, but they increase the production of free radicals within the cell as well - promoting oxidative damage and cell death. However, anthracyclines also inhibit a DNA replication enzyme - the topoisomerase, compromising new DNA production and consequently arresting cell division. There is a whole group of cytotoxic agents with this capability: the topoisomerase-inhibitors. Tubulin-binding drugs like the taxanes (*e.g.*

paclitaxel) bind to microtubules preventing their disassembly and compromising cell shape and function, conditioning mitotic/meiotic processes.

Most limitations of current chemotherapy options are still connected to a reduced effectiveness due to an insufficient concentration at the desired site, or with the above-mentioned side effects of these cytotoxic drugs at healthy tissues. The dosage of administered drug is usually calculated for each patient individually, to avoid excessive concentrations (and consequent toxic effect) at normal cells, while ideally reaching a therapeutic dose and effect at malignant cells, but this is often not the case.[27]

The future of chemotherapy must, therefore, address both these issues with concrete solutions to allow therapists to administrate cytotoxic drugs that will target precisely the cancer cells in a sufficient dose, while maintaining healthy cells safe. The key to this dilemma might be in the drug delivery systems: could we find a system that allows precise administration of drugs to cancer cells?

1.2 Nanomedicine: a novel approach

The urge to improve cancer pharmacologic therapy's effectiveness and undesired effects has led to the rise of numerous new approaches and cooperation between scientific fields. Uniting the knowledge of fields like biology, medicine, engineering, chemistry and physics, nanomedicine rises as a world full of possibilities at a whole new scale. By creating and manipulating materials at the nanoscale, nanomedicine enables, for instance, the design of completely new drug delivery systems – nanocarriers (Figure 5).[28] These systems present completely customizable properties and actions and might be obtained from a wide variety of materials. Given their rather small size, the materials used in this manufacturing process possess specific chemical and physical characteristics, which might be manipulated to improve the bio-distribution or specificity of certain drugs, when loaded in one of those nano-sized drug carriers.

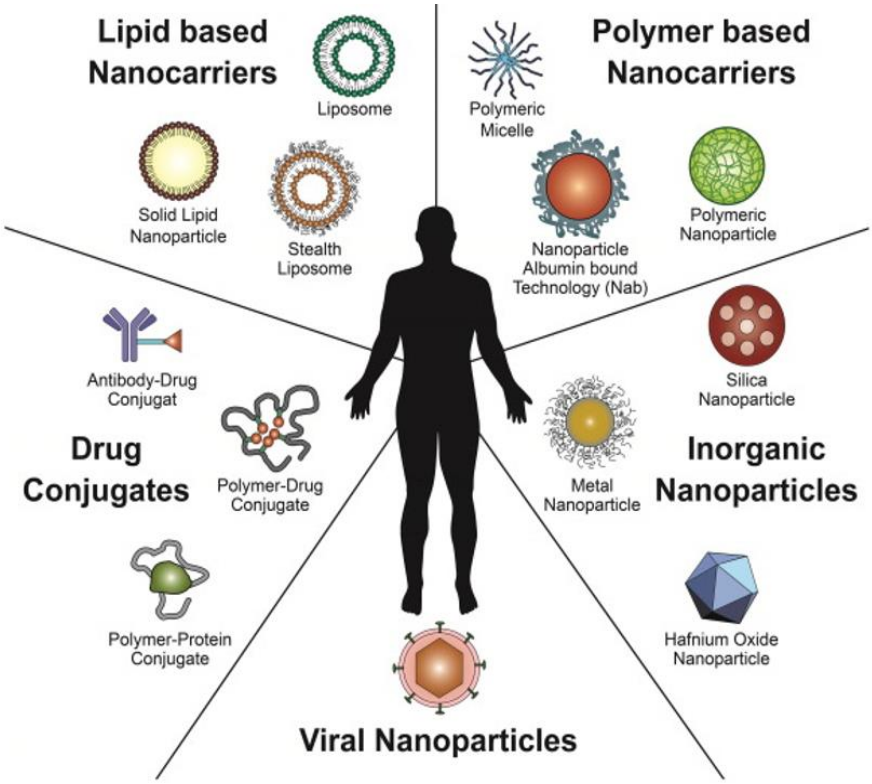

Figure 5 - Examples of nanocarriers and other nanotherapeutic platforms. Reproduced from "Nanomedicine in cancer therapy: Challenges, opportunities, and clinical applications" – Wicki et al. (2015)[29]

Nanocarriers have proven to reduce systemic consequences of cancer therapy by specifically delivering the drugs to the cancerous cells and tissues.[30] By integrating these therapeutic properties with possible diagnostic facilities (by medical imaging), these particles can even be used as theranostic agents. Theranostic agents possess the ability to specifically guide drug release to tumour cells by exhibiting imaging contrast and stimuli-triggered drug release. This means that these agents may act not only as imaging contrast, accumulating at specific locations, but also as a drug carrier, releasing the desired drug only at appropriated sites.[31]

With numerous possible shapes, sizes and compositions, several nanocarriers are currently in the spotlight of cancer therapy innovation. Between those, nanofilms are probably the simplest ones, while nanoparticles have been one of the most intensely described and explored because of their versatility and multiple applications.[29,32]

As already stated, nanocarriers might be obtained from a vast array of materials, from both synthetic and natural origins. However, keeping the therapeutic use in mind, the manufacture of such carriers from natural polymers (biopolymers) might be advantageous, due to their resemblance to the body's own biomolecules and their biodegradable and biocompatible nature.[33]

1.2.1 *Biopolymers for the assembly of nanocarriers*

Biopolymers are macromolecules normally produced by living organisms. Biopolymers like polypeptides and polysaccharides, are constituted by several monomeric units covalently bonded to form a long polymeric chain. The usage of these materials in the synthesis of nanosystems has been widely explored as some of their characteristics (like their biocompatibility or biodegradable nature) are quite attractive for drug delivery intentions. The fact that many of these materials are able to sense and respond to multiple biological signals like pH and certain enzymes, adjusting their structure or function, is also a key characteristic in this application.[34]

1.2.1.1 Polysaccharides

Polysaccharides like chitosan (CH), alginate (ALG), dextran, hyaluronic acid (HA) and cellulose (Figure 6) are commonly used (alone or together with another polysaccharides or biomolecules) in the manufacture of nanocarriers for drug delivery purposes. These molecules, composed by monosaccharides linked by glycosidic bonds, exhibit a close resemblance with many body components, being therefore quite tolerated by the body's defence mechanisms – biocompatibility.[35]

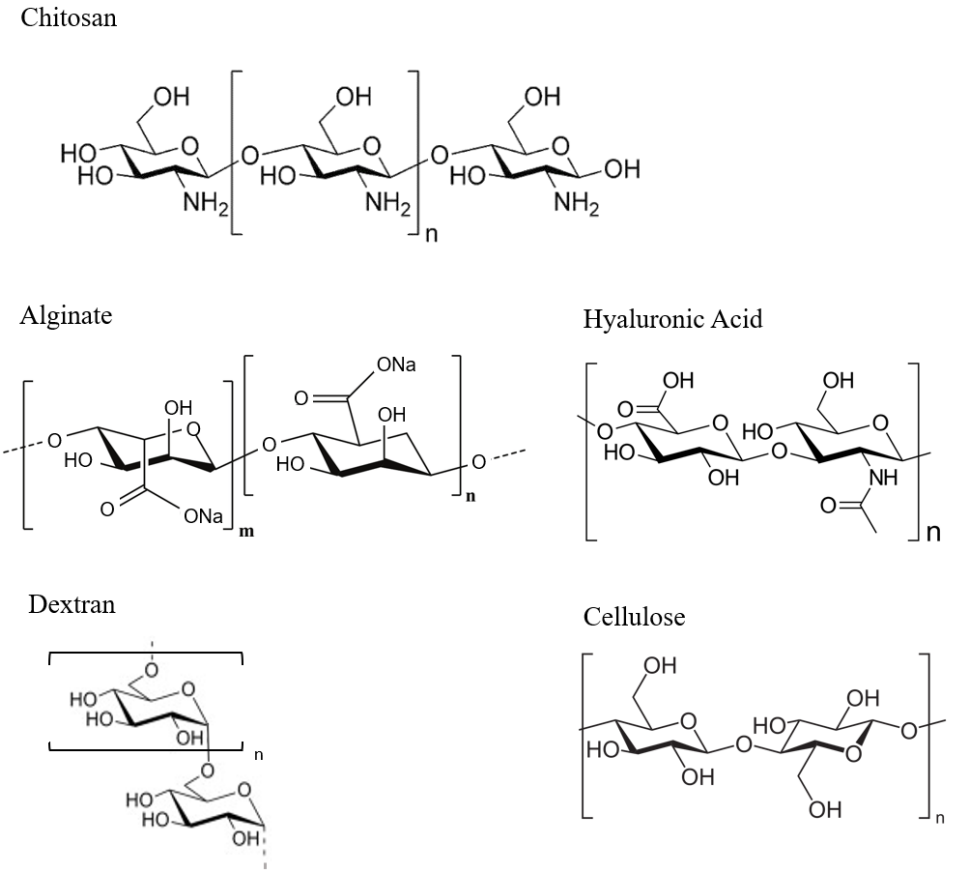

Figure 6 - Molecular structures of chitosan, alginate (in the figure, in the form of sodium alginate), dextran, hyaluronic acid and cellulose.[36–39]

CH is obtained from chitin, the second most abundant polysaccharide in nature (preceded by cellulose) found in the exoskeleton of crustaceans and some insects, and in the cell walls of fungi and bacteria.[40] CH presents cationic properties in aqueous solutions of slightly acid pH, due to the protonation of its amine groups. These polyelectrolyte properties and solubility of CH allow the manipulation of this polymer without resorting to harmful reactants. CH also possesses some rather interesting characteristics for therapeutic uses: biodegradability, non-toxicity, film-forming ability, mucoadhesivity and antimicrobial capacity.[41] Several studies dealing with the production of both CH based nanocapsules and nanofilms for ocular, oral, nasal, dermal, parenteral and transdermal drug delivery, have been described.[42]

ALG is a linear anionic polysaccharide formed by β-D-mannuronic acid and α-L-guluronic acid residues. ALG is extracted from brown seaweeds by alkali extraction

procedures.[43] It is water-soluble and frequently used to form biocompatible hydrogels by cross-linking with divalent cations (like Ca^{2+}). Choosing the right conditions, one can easily obtain matrices with diverse morphologies and decomposition speeds, allowing the sustained release of drugs.[44,45] Alginate is biodegradable, and seems to demonstrate a high mucoadhesion which might be useful in the development of drug delivery systems for mucosal tissues (*e.g.*, nasal).[46]

Dextran is a bacterial exopolysaccharide produced from sucrose. Being a neutral polysaccharide, with simple structure and high-water solubility, it is also commonly used to form hydrogels for drug delivery. Dextran-based hydrogels alone (without additional growth promoters) have shown to promote skin regeneration and neovascularization in dermal wounds.[47] However, this polysaccharide is utilized for coating nanoparticles as well, increasing their biocompatibility in areas like molecular diagnostics and molecular imaging.[48]

HA is an anionic, non-immunogenic and biodegradable polysaccharide that is also largely used as a carrier for drug delivery.[49] HA also seems to improve some drugs' delivery to tumour cells, since it specifically recognizes CD44, a glycoprotein overexpressed in multiple tumour cells' surfaces.[50,51]

Cellulose is usually known as the most abundant polysaccharide in nature. Produced by many living organisms (specially plants and bacteria), it has several applications in the pharmaceutical and biomedical field as transdermal drug delivery systems, hydrogels or even as an excipient in tablet formulations.[52]

1.2.1.2 Polypeptides and proteins

Polypeptides and proteins are polymers of multiple amino acid monomers linked by peptide bonds. The use of proteins as materials for nanocarriers is motivated by their traits of biocompatibility and biodegradability, just like in other classes of biopolymers. However, proteins like albumin, gelatin, silk fibroin or lysozyme also possess their own advantages: their high stability, availability and multiple functional groups that allow multiple interactions with different materials and with the therapeutic compounds themselves.[53]

Albumin is the major plasma protein. It is, therefore, easily available, nontoxic and biodegradable by the body and its uptake is normally exacerbated at inflamed or tumorous tissues. Albumin molecules have high drug-binding capacity, since they possess multiple drug binding sites along their chain, which makes them responsible for the alteration of the pharmacokinetic profile of many drugs. They have also been described as able to cross the blood-brain barrier and deliver drugs to the brain.[54] These traits make albumin a strong candidate for cancer therapy nanocarriers, with BSA (bovine-serum albumin) and HSA (human-serum albumin) nanoparticles production process and compatibility already described and multiple reports on the delivery of anticancer drugs by albumin based nanosystems.[55–57]

Gelatin is commonly used for pharmaceutical, cosmetic and food industry applications. It is obtained from denaturation of collagen, the most abundant mammalian protein, which grants its low immunogenicity. Nanoparticles made from this polymer have been developed for numerous drug delivery purposes, including tuberculosis, HIV and cancer therapeutics.[58]

Silk fibroin is usually produced by some insects for the formation of a cocoon. Its high flexibility, tuneable structure and unique mechanical characteristics grant it a big role in drug delivery systems: from scaffolds to films.[59] Gelatin and silk fibroin have also been used together to produce multi-layered systems for controlled drug release.[60]

Lysozyme obtained from hen egg white (HEWL) is frequently used as a model-protein when studying protein structure and function, specifically formation of amyloid structures.[61] HEWL is water-soluble and possesses widely-described antibacterial properties, with described applications in food-industry and medicine.[62,63]

1.2.2 Layer-by-layer assembly of nanocarriers for drug delivery

The fast pace of innovation in nanotechnology leads to the emerging of new dilemmas. With the developing of novel nanostructures, from new materials and with innovative characteristics, the efficient and consistent manufacture of nanocarriers might present itself as a challenging process.

Multiple approaches for the assembly of multi-layered nanostructures have been described. The layer-by-layer (LbL) assembly methodology is one of the most rapidly strategies for the precise creation of nanocarriers, since it allows the exact control of the size and composition of the materials.[32]

Based on the alternate adsorption of complementary charged species, the LbL assembly of polyelectrolytes on a flat surface was first described by Decher.[64] Starting from a substrate film, charged species with opposed charge are sequentially deposited on top of each other, forming a coating held together usually via electrostatic interactions (Figure 7). This deposition of species might be achieved via dipping or spraying the charged species one by one into the template, and molecules of interest (drugs, imaging substances or others) can be intercalated in between these multiple layers to be gradually released upon degradation of the outer coatings or by diffusion.

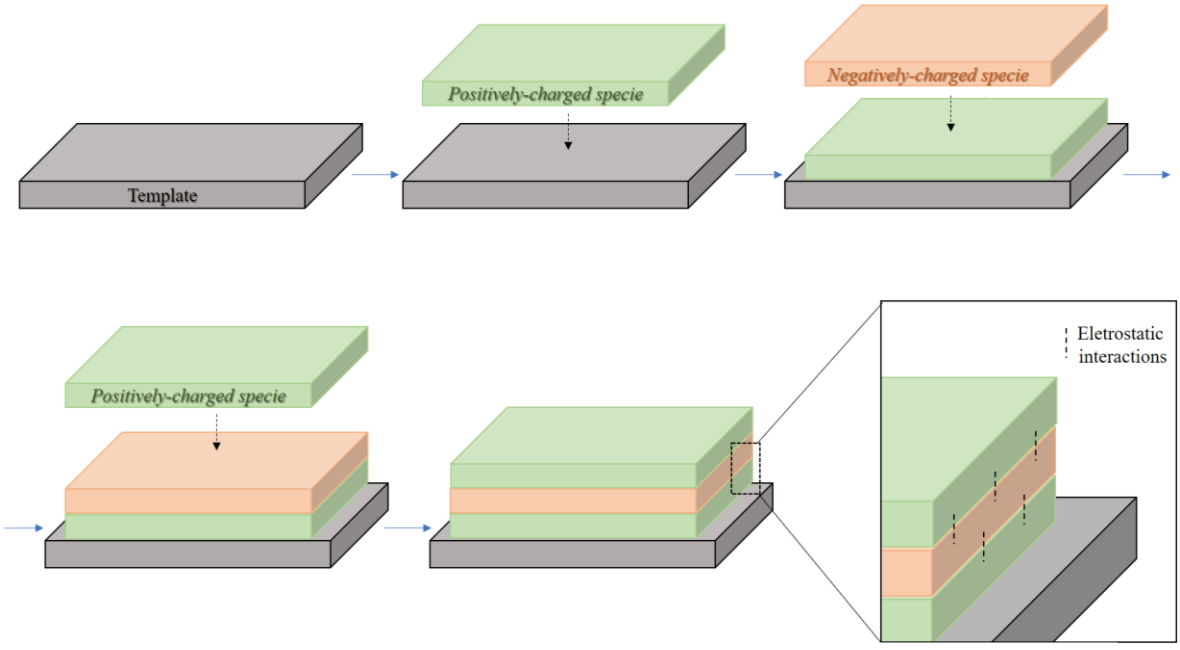

Figure 7 - Schematic representation of the layer-by-layer assembly process. Species of opposed charge are gradually deposited on a template, remaining held together by electrostatic interactions between them

Caruso *et al.*[65] later described the same approach applied to three-dimensional carriers by applying LbL assembly on sacrificial colloidal particles. The colloidal particle (template core) was later selectively removed using adequate solvents, creating a hollow capsule. It is possible to load drugs or other molecules of interest inside these capsules posteriorly (Figure 8). Alternatively, these molecules might be previously incorporated into the template.

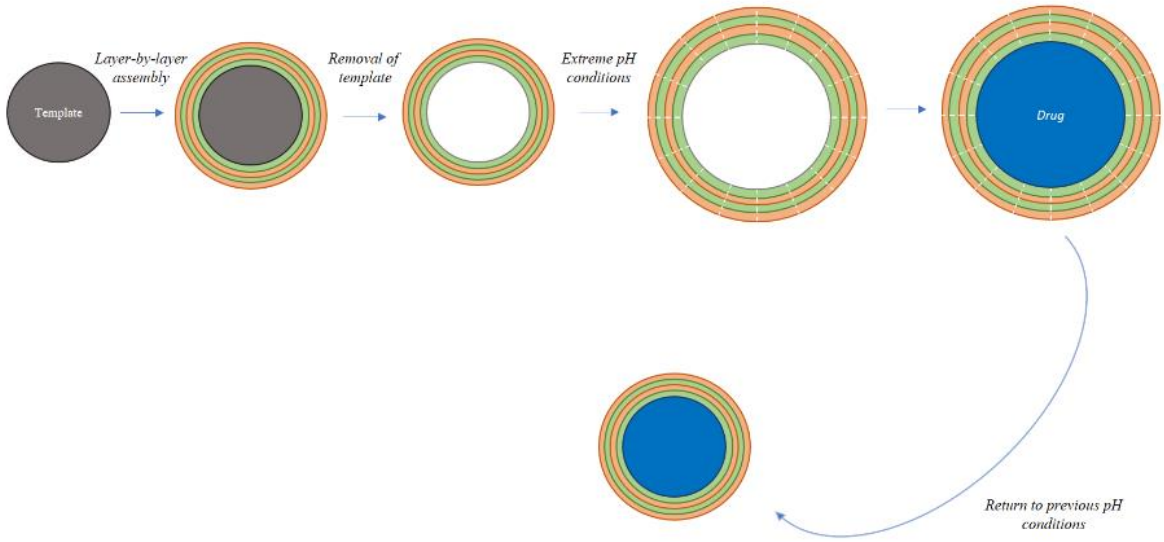

Figure 8 - Schematic representation of LbL assembly of nanocapsules and posterior drug loading. After the outer layers are gradually deposited, the template is removed by exposure to adequate solvents or certain pH values. Extreme pH conditions might also cause the swelling of the resulting hollow capsule, increasing its' permeability and allowing the drug to penetrate. Returning to normal pH conditions will return the capsule to its' previous size, imprisoning the drug inside

Post-assembly drug loading is commonly achieved by intumescing the nanoparticles, increasing their permeability in a reversible way. Extreme medium conditions (like pH or salt concentrations) might cause such changes to these nanocarriers, allowing the desired molecules to penetrate the capsule and be imprisoned inside.

Similarly to what happens in the nanofilms described above, the nanocapsules' characteristics (size, shape, thickness and outer composition) are precisely controlled when they are produced by LbL assembly - molecules of interest might even be included between the multiple layers that compose the capsule. On the other hand, the external surface of these

nanocarriers is also often modified to include molecules that might, for instance, increase the capsule's affinity to certain cells or tissues – targeting.[66]

Overall, this technique presents several advantages: its' simplicity, versatility and reproducibility are a great attractive for the production of nanosystems from multiple materials. As already stated, the layer-by-layer assembly is successfully used to create both nanofilms and nanoparticles. Yet, these are rather different structures with different properties and applications. What are the main differences between these nanocarriers?

1.2.3 Nanofilms

Nanofilms constituted by multiple overlapping layers of polyelectrolytes are frequently obtained by LbL assembly. With very low thickness and possible broad area, these structures have been used as successful drug delivery systems for local applications like wound care and cancer therapy. Due to their possible tuneable properties, including antibacterial activity and inflammation alleviation, their use at the surface of biomedical devices has also been described.[67,68]

The specific characteristics of these films will depend on the polyelectrolytes that compose them, with plentiful possibilities: polysaccharide based, protein based and other biopolymer (like DNA) based nanofilms have been broadly investigated and will be further explored in this section.

1.2.3.1 Polysaccharide-based films

Films obtained from different polysaccharides, like the ones described before, have been used for multiple applications in health care. CH and ALG, being polysaccharides of opposite charge and with intensely described properties, are a common conjugation for the assembly of polysaccharide-based nanofilms.

For instance, Stana *et al*. has described the usage of ALG and *N,N,N*-trimethylchitosan derivative for the LbL-assembly of nanofilms for the controlled release of an anti-inflammatory drug (pentoxifylline) used in the treatment of chronic venous ulceration.[69] Riva *et al*. used CH and ALG for the assembly of nanofilms in a poly(methyl

methacrylate) (PMMA) template layer. An anti-inflammatory drug, APP (4-amino-2-(2-hydroxy-1-decyl)pyrazole-[3,4-d]pyrimidine) was successfully loaded in the film, granting its' potential to eventually be used in the treatment of localized pathologies like inflammatory bowel disease.[70]

Using CH and dextran, Xie *et al*. obtained films by LbL-assembly on graphene oxide nanosheets. Doxorubicin (DOX, an anticancer drug) was included in these nanofilms, resulting in a strong cytotoxicity for MCF-7 cells as shown by *in vitro* experiments.[71] Dextran has also been used with HA to originate films loaded with ibuprofen for surgical sutures or bioadhesives.[72,73] CH-HA films demonstrated antibacterial capacity against *Xylella fastidiosa*.[74]

1.2.3.2 Protein-based films

As already mentioned, proteins (like silk fibroin, albumin and gelatine) might also be used for the assembly of nanocarriers, given their unique characteristics and high versatility and adjustability.

Silk fibroin has been widely exploited as a material for coatings of biomedical devices or as drug delivery systems, including nanofilms.[75,76] The potential of silk fibroin films as sustained release systems was explored using horse-radish peroxidase and lysozyme as model compounds.[77] The release behaviour of molecules from films of gelatin and silk fibroin was tested using trypan blue, fluorescein isothiocyanate (FITC)-inulin and FITC-BSA. This release was not influenced by the size of these molecules, and these films revealed potential for controllable drug release.[60] Mohanta *et al*. described the usage of an aqueous dispersion of BSA nanoparticles together with CH to form nanofilms capable of carrying and selectively releasing drugs given a certain pH-stimulus.[78]

Using another peptide, poly(L-lysine) (PLL), and three different three-dimensional DNA molecules, Cho *et al*. described the layer-by-layer assembly of nanofilms with distinct tuneable characteristics (release profiles and structure stability in serum medium) depending on the chosen DNA structure.[67] PLL was also used together with poly(L-glutamic-acid) (PLGA) to investigate the resulting film's ability to contain and release small charged

molecules. When loaded with antibiotics (cefazoline or gentamicin), the PLL-PLGA nanofilms revealed adjustable antimicrobial activity against *Staphylococcus aureus*.[68]

1.2.4 Nanoparticles

Although nanofilms constitute a remarkable drug carrier for local administration, their systemic usage is not viable. Their three-dimensional counterparts, on the other hand, might be easily administered via intravenous injection to reach every cell in the body through the bloodstream, given their reduced size and high biodistribution. This has made nanoparticles a topic of increasing interested in Nanomedicine, namely for the systemic delivery of drugs.

These spherical nanocarriers have the potential to be used as drug carriers to reach virtually any cell, release the contained molecules and, when obtained from biodegradable materials, be degraded by the body's metabolism without traces of toxic metabolites. While this might sound ideal for most systemic pharmacologic treatments, this is not the case in most of the oncologic regimens. The highest goal of cancer therapy is much more complex than that: ideally, the drug must be released and affect exclusively the cancer cells that might be located anywhere at the organism, leaving all the healthy cells as intact as possible.

The key to using these nanosystems as a drug carrier for cancer therapy will therefore reside in these carriers' capacity to specifically target cancer cells. An alternative approach could consist in limiting the release of the cytotoxic drugs by the capsules only at the desired sites, by the application of localized external stimuli.

1.2.4.1 Layer-by-layer assembly of nanoparticles

Spherical nanocarriers might be obtained from a vast array of polymers, just like nanofilms, using LbL assembly. Donath *et al*. first described the alternating deposition of polymers of opposite charge on a three-dimensional template: a melamine formaldehyde colloidal particle. The template was later dissolved in acidic solution, leaving a hollow capsule of poly(allylamine hydrochloride) (PAH) and poly(styrene sulfonate) (PSS).[79] Since

then, many different templates have been successfully used for this purpose: polystyrene particles, poly(lactic acid) (PLA), silicon dioxide (SiO_2), microorganisms and inorganic crystals (like $MnCO_3$ and $CaCO_3$).[80]

The polysaccharides and polypeptides described before for the manufacture of nanofilms are also the most common materials used on the design of biodegradable nanocapsules. CH and ALG is a typical combination, used in several studies for the assembly of capsules from various templates and to contain diverse molecules.[81,82] However, other combinations like gelatine and ALG have also been described, like in the work of Chen *et al.* with artemisin (an anticancer drug).[83] In another study, paclitaxel (PTX), an antiproliferative drug with hydrophobic behaviour, has been successfully encapsulated in capsules of HA and CH derivatives, achieving a significant decrease on the viability and proliferation of MDA MB 231 breast cancer cells.[84]

The usage of biopolymers in the synthesis of these nanocarriers will grant them their high biocompatibility and versatility. However, these "building blocks" might also hold the key for the precise release of drugs, given their intrinsic characteristics.

1.2.4.2 Stimuli-responsive nanocarriers

Since these nanoparticles have the ability to reach nearly every cell in the human body through the bloodstream, one of the answers to the dilemma of precise administration of drugs might be in the engineering of nanosystems in order to limit the release of their loads only when a certain stimulus is applied. These stimuli-responsive carriers will keep their cargo inside unless the external stimuli trigger their opening, allowing therapists to circumscribe the drug effect to the local of the stimulus (*e.g.* radiation). Alternatively, therapists might be able to predict the environment at which they would like the nanoparticles to release the desired drug (*e.g.* certain pH values).

Enzyme-responsive systems

Several nanoparticles fall into the category of enzyme-responsive systems. These carriers depend exclusively on the gradual enzymatic degradation of the outer layers of

polyelectrolytes for a controlled release of the drugs intercalated between them or contained inside the capsule. One can therefore control the release speed of the drugs by varying the thickness of the shell or its constituents: thinner shells will be degraded more rapidly than thicker ones, and shells including synthetic polymers will be degraded slower than shells made purely of natural biopolymers.[85] Szarpak *et al*., for instance, have tested the enzymatic degradation of hyaluronic acid (HA) and PLL capsules, proving their potential as drug carriers. Itoh *et al*. researched the enzymatic degradation of CH-dextran nanoparticles by chitosanase, testing the effect of manipulating the surface's charge in this process.[86,87]

Even though these enzyme-responsive nanoparticles have been quite explored for drug delivery, they are independent of an external trigger for the release of their cargo, making it difficult to accurately predict the initial time of release and to limit the effect to certain areas.

pH sensitive systems

Nanosystems responsive to pH present an interesting approach for cancer therapy. Since cancer tissues show a pH of under 6.8 due to their low perfusion and high metabolic rates (while most normal tissues have pH values around 7.4), capsules that have the capacity to release their cargo at acidic environments might be the key for precise therapeutics.[88] Interestingly, pH changes are dependent on the capsules constituents and usually reversible, being normally used in the drug-loading process during these capsule's assembly.

The release of the drugs from these carriers is based on the accumulation of charges on the polyelectrolytes, once they are exposed to pH values that cause protonation. This accumulation increases the repulsion between polyelectrolyte molecules, causing the capsule's permeability to increase.[80] This process is normally reversible, as long as the capsule is exposed to the previous pH values. Imoto *et al*. synthetized pH-responsive nanocapsules of CH and poly(G-glutamic acid), achieving the release of the encapsulated drugs at acidic pH (and little to no release at alkaline and neutral pH).[89] Cuomo *et al*. have tested the behaviour of both CH and ALG at different pH values by synthetizing capsules with outer layers of each of these polymers.[90]

Nanocapsules sensitive to pH changes might therefore constitute an important approach for cancer therapy. Nevertheless, they might also be an interesting new therapeutic option in diseases of the digestive tract, for instance, due to the known pH variation along the digestive tube.

Radiation sensitive systems

Radiation sensitive systems normally contain a radiation (*e.g.* UV) responsive component which will damage the carrier's shell when exposed to UV light. Koo *et al.*[91] described the synthesis of capsules with photoacid generators (PAGs) which would, when exposed to UV light, cause the release of protons (and consequently the decrease of the medium's pH) leading to the swelling and increased permeability of the capsules. Prolonged exposure to UV radiation caused the rupture of the capsules. However, the application of UV radiation to biological samples is questionable due to its known mutagenic potential and damage to living cells.[92]

Near-infrared (NIR) light, on the other hand, results in less harm to these cells and has a stronger capacity to penetrate tissues. Muñoz-Javier *et al.*[93] have described the usage of polyelectrolyte capsules with metal nanoparticles in their shells, with fluorescent cargo. The heating of the carriers, induced by the exposure to NIR light, led to the complete rupture of the capsules with release of the fluorescent cargo to the cytosol. Moreover, the opening of the capsules achieved at moderate light intensities did not affect cellular viability and metabolism.

1.2.5 Targeted delivery of drugs by functionalized nanocarriers

The targeted delivery of a drug to specific cells or tissues might also be achieved by the functionalization of these nanoparticles. By including specific binders in the nanocarriers' outer layers, it is possible to actively target these nanocarriers for cancer cells, increasing their accumulation on cancer tissues and thus minimizing the systemic spread of such carriers and reducing the toxicity to healthy tissues.[94] Cancer cells normally overexpress certain molecules at their membrane, including numerous receptors. These

receptors are usually present in many healthy cells, but they exist in aberrantly high concentration on cancer cells. Therefore, the knowledge of which receptors might be overexpressed allows therapists to select specific binders that will make nanoparticles more prone to accumulate at cancer tissues (Figure 9).

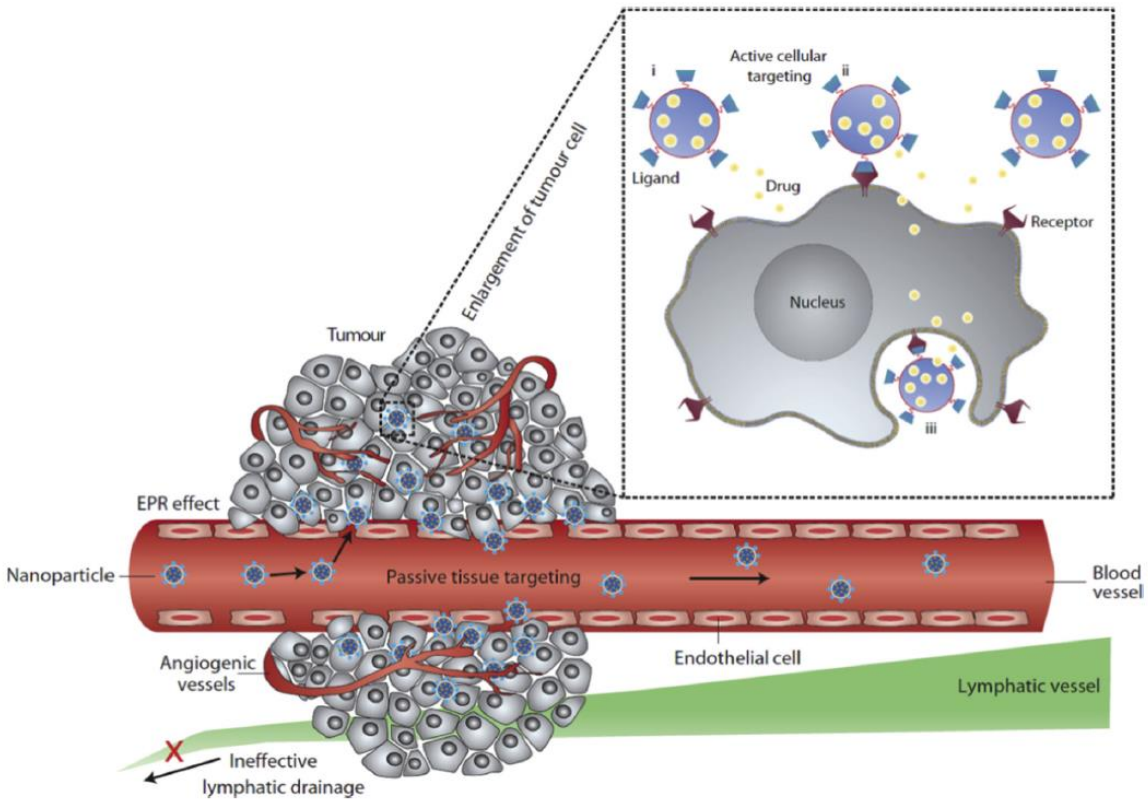

Figure 9 – Active cellular targeting allows the accumulation of nanoparticles at specific sites. These will either (i) release their content near to the cancer cells; (ii) bind to the membrane and release their content inside the cancer cells or (iii) be internalized into these cells. Reproduced from "Advanced targeted therapies in cancer: Drug nanocarriers, the future of chemotherapy" – Pérez-Herrero et al. (2015)[95]

The most common binders for targeting purposes are proteins (like antibodies, receptors and peptides), which relay on the immune system's complementary elements (antigen/antibody) to achieve the desired specificity. However, other molecules (like carbohydrates) have also been successfully applied for targeting applications.[95]

Kamphuis *et al.* have used humanized A33 monoclonal antibody (huA33mAb) at the surface of nanocapsules obtained through LbL assembly, thus achieving specific binding of

these carriers to the cancer cells expressing the target antigen. This highly specific targeting was observed even when the target colorectal cancer cells constituted less than 0.1% of the cell population, while the nonspecific binding was insignificant (under 0.5%).[96] Another noteworthy work is the functionalization of nanocapsules loaded with rapamycin by the use of EGFR (epidermal growth factor receptor)-antibody.[94] EGFR is commonly found overexpressed in many tumours, including the MCF-7 breast cancer cells used in this experiment. The antibody-decorated nanoparticles showed increased anticancer activity when compared against antibody-free particles or free rapamycin.[94] Similar results were obtained by Cirstoiu-Hapca *et al.* using antibodies for HER2 (a membrane receptor from the EGFR family commonly overexpressed in breast and ovarian cancers) in the surface of PTX-loaded nanoparticles.[97]

As already stated, HA is a biopolymer used in the assembly of nanocarriers, with high biocompatibility. However, it might as well act as a binder for targeting in cancer therapy, since it possesses the ability to specifically bind to the glycoprotein CD44 receptor, which is frequently overexpressed in certain cancer cells, like the SCC7 (squamous cell carcinoma) cells. The HA-nanoparticles developed by Choi *et al.* circulated for two days in the bloodstream of mice and successfully accumulated at tumour sites, according to the *in vivo* studies performed.[98]

Folic acid and folate are also commonly used as targeting ligands since folate receptors are frequently overexpressed in the cells of many epithelial (like ovary, lung, mammary gland and prostate cancer) and hematologic cancers, and in sarcomas. Parveen *et al*. have used CH nanoparticles loaded with DOX and conjugated with folic acid for the targeted delivery of the drug to retinoblastoma.[99] Liang *et al.* prepared PLGA-PEG (polyethylene-glycol) nanocapsules with folate as targeting ligand. The capsules were loaded with PTX and showed increased cytotoxicity against HEC-1A (human endometrial adenocarcinoma) cancer cells.[100] Other molecules have also been used for specific targeting applications, like albumin,[101] biotin[102] and transferrin.[103]

The use of all these molecules as ligands for nanoparticles is allowing the therapists to deliver the drugs to cancer cells with increased specificity, eventually circumventing or decreasing potential systemic or unspecific side effects *in vivo*.

1.3 Aims of the Present Study

Given the increasing interest in nanomedicine, specifically in the use of nanocarriers for drug delivery purposes, and their potential to change the chemotherapy paradigm (increasing effectivity and specificity, while reducing undesired side-effects), the development, production and characterization of new nanocarriers becomes extremely relevant.

Spherical nanocarriers with high versatility and multiple adjustable characteristics, are particularly interesting due to their potential to be used as a systemic (yet specific) approach to cancer therapy, since they can be administrated intravenously. The possibility to manufacture these nanocarriers from biopolymers with biodegradable and biocompatible nature, finely adjusting their characteristics (like size or number of layers) and controlling the release of the encapsulated drug will be the core of the present dissertation project.

Specifically, the present study consists in the fabrication and characterization of nanoparticles for cancer therapy by LbL assembly of different biopolymers, namely ALG, CH and protein nanofibrils, on SiO_2 spherical templates loaded with a model-drug, *viz.* curcumin (CUR), as summarized in Figure 10.

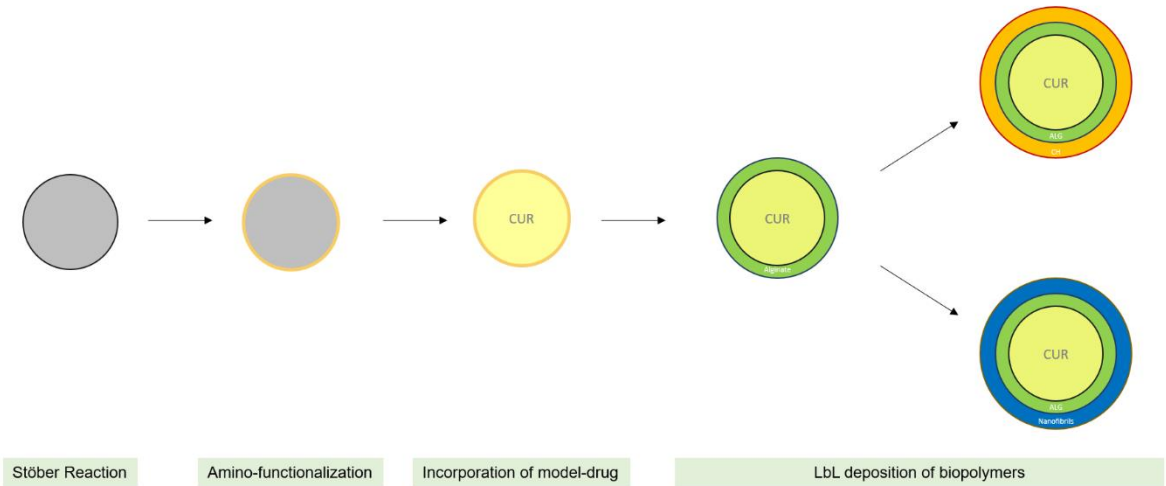

Figure 10 - Schematic representation of the assembly process used to obtain the nanoparticles investigated in this study. First, SiO_2 particles will be synthetized through the Stöber reaction and have their surface amino-functionalized. The incorporation of CUR will later be performed, followed by the LbL deposition of biopolymers (ALG, CH and nanofibrils).

Curcumin (Figure 11) is a bioactive compound obtained from the rhizome of *Curcuma longa*. It is the bright yellow pigment present in the turmeric spice, which has been used in Asian medicine and cuisine for centuries. Several studies have pointed curcumin as an option for inflammation, oxidative stress or diabetes, but the oncological perspective is particularly appellative: CUR is described as a possible chemotherapeutic and chemopreventive agent, damaging cancer cells and simultaneously protecting normal cells.[104] CUR's activation of PPAR-γ (a nuclear receptor involved in cell cycle control and proliferation) in rat hepatic stellate cells and Moser cells (a human colon cancer cell line) has been proven to reduce these cells' division, inhibiting their proliferation.[105,106] However, CUR's anti-cancer effect is mostly attributed to its' inhibitory effect on NF-κB, a transcription factor involved in cell proliferation.[107]

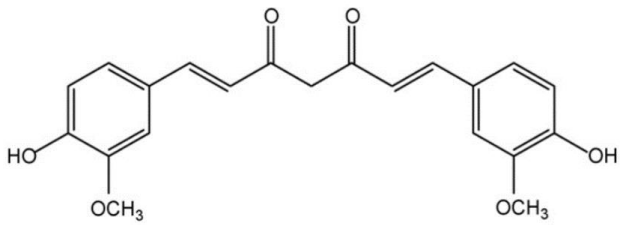

Figure 11 - Chemical structure of curcumin. Reproduced from Epstein et al. (2009) [104]

The use of CUR on therapeutics is still quite limited due to its' very low bioavailability, fast metabolization and low solubility in water. Including CUR in a nanocarrier could potentially help circumvent these intrinsic characteristics of the molecule by increasing its' bioavailability and improving its' pharmacokinetics.

Protein nanofibrils (also known as amyloid fibrils) are proteic structures with fibrillar shape composed by several stacked *β*-sheets. Inducing the fibrillation of a native protein depends on the disruption of intramolecular hydrogen bonds by a variety of conditions - in this case, fibrillation will be induced in HEWL by using a deep eutectic solvent (DES), cholinium chloride:acetic acid, at high temperatures and acidic pH. The resulting nanofibrils are highly stable and normally possess diameters in the nanoscale (10-100 nm), variable length and high tensile strength. Nanofibrils can be used to mechanically reinforce the

particle or to serve as an additional way to allow the introduction of new functionalities to the nanoparticles containing anticancer drugs.

The nanocarriers resulting from this work were submitted to a drug-release test, in order to understand the release profile of the incorporated model-drug, *i.e*. CUR. Later, *in vitro* cytotoxicity tests in HepG2 cell line were performed to evaluate their impact and possible cytotoxic effect on human liver cancer cells.

2 Experimental Procedure

The following chapter will comprise a thorough description of the materials and experimental procedures followed throughout the work included in this study. The characterization techniques used to characterize both the starting materials and the materials prepared in this study, namely the multi-layered systems, are also described in this section.

2.1 Reagents and cells

Chitosan (CH, molecular weight of 15 kDa, deacetylation degree > 85%) was supplied by Polysciences, Inc. Alginate (ALG, alginic acid sodium salt from brown algae), tetraethoxysilane (TEOS, purity ≥ 98.5%), (3-aminopropyl)triethoxysilane (APTES, purity ≥ 98%), curcumin (CUR, purity ≥ 65%), choline chloride (purity ≥ 98%), glycine (purity ≥ 98.5%), lysozyme from hen egg white (HEWL, ≈ 70000 U mg^{-1} activity) and Thioflavin-T were provided from Sigma-Aldrich. Ammonia solution 25% was obtained from LabKem. Ultrapure water was obtained through a Milli-Q Simplicity UV Type system from Millipore. Acetic acid (glacial, > 99% purity) was provided by Chem-Lab and anhydrous absolute ethanol was supplied by Carlo Erba Dasigroup.

The human liver cancer cell line (HepG2) was obtained from the European Collection of Authenticated Cell Cultures (ECACC) and supplied by Sigma Aldrich (St. Louis, MO, USA). Phosphate buffered solution (PBS, pH 7.2), Dulbecco's Modified Eagle's Medium (DMEM), fetal bovine serum, L-glutamine, penicillin/streptomycin and fungizone were purchased from Gibco. Dimethyl sulfoxide (DMSO, purity ≥ 99.5%) and 3-(4,5-dimethylthiazolyl-2)-2,5-diphenyltetrazolium bromide (MTT, 98%) were supplied by Sigma-Aldrich.

2.2 Preparation of silica templates

The assembly of spherical multi-layered nanosystems from biopolymers depends on the utilization of round templates as a starting point. In the present work, the SiO_2 templates were obtained by the so-called Stöber method.[108] Therefore, and considering the work of Pinto *et al.*,[109] 2.25 mL of ultrapure water and 2.25 mL of TEOS were added to five Erlenmeyer flasks. Different volumes (0.55, 0.75, 0.95, 1.15 and 1.90 mL) of ammonia were posteriorly added to each flask, to obtain nanoparticles of different sizes (depending on the ammonia concentration at the final reaction volume (0.15, 0.20, 0.25, 0.30 and 0.50 M, respectively). Ethanol was then added until all reaction mixtures had a total volume of 50 mL. All flasks were left under moderate stirring for 24 hours at room temperature. The obtained silica particles were then collected by centrifugation and washed once in ethanol and twice in ultrapure water. Lastly, the suspension was left to dry for 24 hours in an oven at 50 ºC.

The morphology of the obtained SiO_2 templates was then investigated by scanning electron microscopy (SEM, see section 2.8.3) and their average size was analysed by ImageJ Software. Zeta-potential analysis was also performed (see section 2.8.2).

2.2.1 Functionalization of silica templates

Considering the work described by Liu *et al.*,[110] the SiO_2 templates obtained previously were functionalized with amino-groups by reaction with APTES. To achieve this, 100 mg of these templates were first dispersed in 20 mL of ethanol. Total dispersion of the particles was assured by placing the suspension in an ultrasonic bath for 30 minutes. 50 µL of APTES were then added to the mixture, which was left under moderate magnetic stirring for 12 hours.

The amino-modified silica particles were posteriorly washed five times with ethanol to remove any leftover of APTES. This was achieved by centrifuging the suspension (at 6000 rpm for 30 minutes), replacing the supernatant and re-dispersing the silica (via an ultrasonic bath).

The obtained particles were re-dispersed in ultrapure water and stored in the refrigerator. Their morphology and size were analysed via SEM/ImageJ Software and their zeta-potential measured.

2.3 Incorporation of model-drug

The process for the incorporation of the model-drug (curcumin, CUR) on the amino-modified templates is based on the works of Kim *et al.*[111] and Taebnia *et al.*[112] Briefly, 4 mg of CUR were dissolved in 2 mL of ethanol and 40 mg of the silica templates were then added. The mixture was left under moderate stirring at room temperature for 24 hours.

The resulting CUR-loaded templates were then washed twice with ultrapure water and finally dispersed in an acetic acid aqueous solution 1% (v/v), in order to begin the deposition of the biopolymeric layers.

The supernatants from the above-mentioned washing processes were collected and analysed via UV-Vis spectroscopy, allowing the determination of the efficiency of the incorporation process (see section 2.8.4.1).

SEM and ImageJ Software were used to investigate possible morphologic or dimensional changes on the nanoparticles, and the zeta-potential measurement was performed.

2.4 Preparation of lysozyme nanofibrils

Lysozyme nanofibrils (LNFs) were obtained by following the procedure described by Silva *et al.*[113] A deep eutectic solvent (DES) was first prepared by mixing cholinium chloride and acetic acid in a 1:1 mol proportion. HEWL was dissolved (2 $mg.mL^{-1}$) in an aqueous solution of 10 mM HCl (pH=2) with 20 mM glycine and 5% (v/v) of the previously prepared DES. This mixture was incubated overnight in an oil bath (at 70 ºC) under moderate magnetic stirring.

The obtained LNFs were separated by centrifugation at 15000 rpm for 30 minutes and washed four times with ultrapure water. The supernatant from this washing process was

collected and analysed via UV-Vis spectroscopy to determine the percentage of fibrillated protein (see section 2.8.4.2). The LNFs' amyloid structure was then investigated by fluorimetry assays using Thioflavin-T as fluorescent dye (see section 2.8.5).

Scanning transmission electron microscopy (STEM) observation of the morphology and size of the nanofibrils, and pH and zeta-potential measurements were also carried out on the LNFs suspension, which was then kept in the refrigerator until further use.

2.5 Preparation of multi-layered systems

The assembly of the multi-layered systems by LbL assembly was preceded by the preparation of the polyelectrolytes (CH and ALG biopolymers) aqueous solutions with a concentration of 2 $mg.mL^{-1}$. CH was dissolved in an aqueous solution of acetic acid 1% (v/v), while ALG was dissolved in ultrapure water. The pH values were verified and adjusted to keep ALG at a pH value of 6, and CH at a pH value of 3.

A total of 15 mg of the CUR-loaded templates were centrifuged from the original suspension and re-dispersed in 10 mL of an aqueous solution of acetic acid 1% (v/v), using an ultrasound bath for 30 minutes.

The assembly of biopolymers began by the dropwise addition of 5 mL of ALG to the CUR-loaded templates in acetic acid. The mixture, kept under moderate stirring for 15 minutes, was later washed three times with ultrapure water to remove the excess of free polyelectrolyte. This washing process consisted on the centrifugation of the sample at 6000 rpm for 30 minutes, followed by the substitution of the supernatant with ultrapure water. The particles were regularly exposed to an ultrasound bath to promote total redispersion.

The depositions of CH and LNFs were similar to the deposition of ALG, involving the same steps described above. However, the final washing processes were carried out using an aqueous solution of acetic acid 1% (v/v).

On a preliminary test, ALG and CH were alternately deposited on the outer layers of the nanosystems until a total of 5 layers was achieved (ALG/CH/ALG/CH/ALG). Later, two-layered particles were prepared (ALG/CH and ALG/LNFs) in order to allow the study of the potential of LNFs as a biopolymeric material for LbL assembly.

Zeta-potential measurements were carried out in between every deposition of polyelectrolytes, to confirm the inversion of the particle's surface potential and, therefore, confirm the deposition of each layer of biopolymer on top of the previous one.

The SEM analysis of the multi-layered particles was performed to investigate the morphological and dimensional changes induced by the deposition of polysaccharides and LNFs.

2.6 Drug release assay

The procedure used to evaluate the release of CUR from the nanosystems was performed considering the work of Taebnia *et al.*[112] For this assay, 3 mg of the particles were dispersed in 15 mL of PBS. The resulting sample was left on an oil bath at 37 ºC under magnetic stirring (200 rpm) for 24 hours.

A volume of 1 mL of the medium was collected at regular time-intervals (0.5, 1, 1.5, 2, 3, 4, 6 and 24 hours) and replaced with the same volume of fresh PBS. The samples collected were centrifuged for 20 minutes at 6000 rpm and analysed via UV-Vis spectroscopy to determine the concentration of released CUR present in the sample (see section 2.8.4.3).

2.7 *In vitro* cytotoxicity assays

2.7.1 Cell culture maintenance

HepG2 cells were cultured in Dulbecco's Modified Eagle Medium (DMEM) supplemented with 10% fetal bovine serum, 1% fungizone, 1% glutamine, 1% sodium pyruvate and 1% penicillin/streptomycin and maintained in an incubator at 37 °C and 5% CO_2. The cells were tripsinized and replated every 3-4 days (when confluency was nearly 80%).

2.7.2 MTT assay

The cytotoxicity potential of the materials was evaluated in human liver cancer cell line (HepG2 cells) by using the MTT assay[114] which involves the conversion of the water soluble MTT to an insoluble formazan. HepG2 cells were seeded at 6000 cells per well in a 96-well plate. After a period of 24 hours of incubation at 37 °C and 5% CO_2, the medium was replaced with the suspensions of nanoparticles: (i) ALG/CH, (ii) ALG/LNFs, (iii) SiO_2+CUR and (iv) bare SiO_2, in fresh DMEM. Five different concentrations (12.5, 25, 50, 100 and 200 $\mu g.mL^{-1}$) of particles were tested for each sample.

The cells were exposed to these suspensions for periods of either 24 and 48 hours, after which 50 µL of MTT (1 $mg.mL^{-1}$) were added to each well and left to incubate for 4 hours at 37 ºC and 5% CO_2.

Posteriorly, the medium was removed from every well and replaced with 150 µL of DMSO. The plates were then left in an orbital shaker for 2 hours, protected from light. The percentage of inhibition was calculated by recording the absorbance of each well at 570 nm (see section 2.8.4.4).

2.8 Characterization techniques

Along the experimental procedures described, particles and materials were characterized using multiple techniques. The starting materials (CH and ALG solutions and LNFs) were subjected to pH and zeta-potential analysis before their utilization. LNFs were also observed by STEM to evaluate their structural integrity and nanofibrillar shape.

The SiO_2 particles had their pH and zeta-potential values regularly measured along the procedure. Since LbL assembly relays on the electrostatic interactions between oppositely-charged materials, the inversion of the zeta-potential might be used to infer the deposition of each layer on the particles. Therefore, these measurements were carried out in between every deposition of biopolymers (and after multiple washes), on suspensions of the particles used.

A frequent analysis of the nanosystems morphology and size was also carried out through SEM visualization and ImageJ Software analysis.

UV-Vis spectroscopy allowed the determination of CUR incorporation by the templates and CUR release by the multi-layered systems. The fibrillation percentage of the lysozyme was also evaluated by UV-Vis spectroscopy, while the amyloid structure was confirmed by fluorimetry assay.

2.8.1 pH measurement

pH measurements of the samples were performed at room temperature, using a Hanna Instruments HI 2211 pH/ORP Meter.

2.8.2 Zeta-potential measurement

The results presented for the zeta-potential values are the mean of three consecutive measurements carried out at 25 ºC on a Zetasizer Nano-ZS from Malvern Instruments. Samples were prepared by diluting 50 μL of the analyte in 1 mL of either 1% (v/v) acetic acid aqueous solution (for APTES-modified silica, CH solution and particles with CH or LNFs as the outer layer); or 1 mL of ultrapure water (for ALG solution, free LNFs and particles in which the outer layer is ALG).

2.8.3 Scanning Electron Microscopy (SEM)

SEM and STEM images were obtained by a Hitachi SU-70 microscope operating at either 8 or 15 kV. Samples for SEM were prepared by dilution of 20 μL of each analyte in 1 mL of ultrapure water. A single drop of this suspension was then deposited on top of a glass fragment fixed in a SEM stub by carbon tape, and air dried at room temperature. STEM samples of LNFs were prepared by dipping the STEM grid on the LNFs' suspension and allowing it to dry overnight at room temperature.

Average particle size was determined using ImageJ Software for the measuring of a minimum of 100 particles from each of the randomly obtained SEM micrographs.

2.8.4 UV-Vis spectroscopy and Fluorimetry

A BioTek Synergy HT Microplate Reader was used for the absorbance measurements of the microplates from the MTT assay. A Shimadzu UV-1800 was used for all the other absorbance measurements carried out under this study.

2.8.4.1 Incorporation of model-drug

Regarding the supernatants of the CUR loading process, the absorbance was measured at 430 nm, and the results analysed by using a calibration curve ($y = 0.0806x + 0.0536$, $R^2 = 0.9945$) determined using known concentrations of ethanolic solutions of CUR. The incorporation of CUR in the templates was calculated using the following equation:

$$\text{Incorporation (\%)} = \frac{\text{Total mass of curcumin} - \text{Mass of curcumin at supernatant}}{\text{Total mass of curcumin}} \times 100$$

2.8.4.2 Fibrillation percentage

The absorbance of the supernatant collected after the fibrillation process was measured at 276 nm. These results were analysed using a calibration curve ($y = 3.365x - 0.0628$, $R^2 = 0.9866$) of known concentrations of aqueous solutions of lysozyme, and allow us to determine the percentage of fibrillation by the following equation:

$$\text{Fibrillation (\%)} = \frac{\text{Total mass of lysozyme} - \text{Mass of lysozyme at supernatant}}{\text{Total mass of lysozyme}} \times 100$$

2.8.4.3 Fluorimetry

A Horiba Jobin Yvon Fluoromax-4 fluorimeter was used to evaluate the fluorescence of the LNFs suspensions marked with Thioflavin-T.

2.8.4.4 Drug-release assay

The concentration of CUR released at each time-interval was evaluated by measuring the absorbance of each sample at 430 nm, and the results analysed by using a calibration curve ($y = 0.0806x + 0.0536$, $R^2 = 0.9945$), determined using known concentrations of ethanolic solutions of CUR. The cumulative release of CUR by the nanosystems was calculated using the following equation:

$$\text{Cumulative release (\%)} = \frac{(C_n \times V_{total}) + \sum(C_{n-1} \times 1)}{m_{total\ CUR}} \times 100$$

In which C_n is the concentration of CUR in the solution at a given moment (n) as measured by UV-Vis spectroscopy; V_{total} is the total volume of PBS used in the assay; $\sum(C_{n-1} \times 1)$ is the sum of all the previous concentrations of CUR measured at the UV-Vis until the moment n; and $m_{total\ CUR}$ is the total mass of CUR incorporated in the nanoparticles (as assessed in section 2.8.4.1).

2.8.4.5 MTT assay

The percentage of inhibition was calculated by recording the absorbance of each well at 570 nm and by comparison against the negative controls, using the formula:

$$\text{Inhibition (\%)} = \frac{\text{Absorbance of the well}}{\text{Absorbance of the negative control}} \times 100$$

2.9 Statistical Analysis

The statistical analysis included in this work was performed using an unpaired *t-test* to calculate the *p-value* and to investigate the statistical differences. *P-values* of 0.05 or less were considered statistically significant.

3 Results and Discussion

In the present study, LbL assembled nanoparticles consisting of different biopolymers, namely alginate, chitosan and protein nanofibrils, on SiO_2 spherical templates loaded with a model-drug, *viz*. curcumin, were fabricated, characterized and their *in vitro* cytotoxicity towards human liver cancer HepG2 cell line evaluated.

3.1 Preparation of silica templates

The process for the synthesis of spherical SiO_2 particles described by Stöber *et al.* in 1968 is still one of the go-to strategies for reliable manufacture of particles of controllable and uniform size. This approach relies on the hydrolysis and condensation of TEOS in ethanolic solution catalysed by the presence of ammonia.[108] As reported by Pinto *et al.*, varying the ammonia concentration in the reactional mixture will result in particles of different sizes, *i.e.*, higher concentrations will result in larger spheres, while lower concentrations will result in smaller particles.[109]

In this work, SiO_2 nanoparticles were synthetized by the Stöber method using increasing concentrations of ammonia, namely 0.15, 0.20, 0.25, 0.30 and 0.50 M. The resulting nanoparticles presented the expected spherical shape, as depicted in Figure 12. Regardless of the size, all particles observed through SEM were individualized and dispersed, showing a smooth surface.

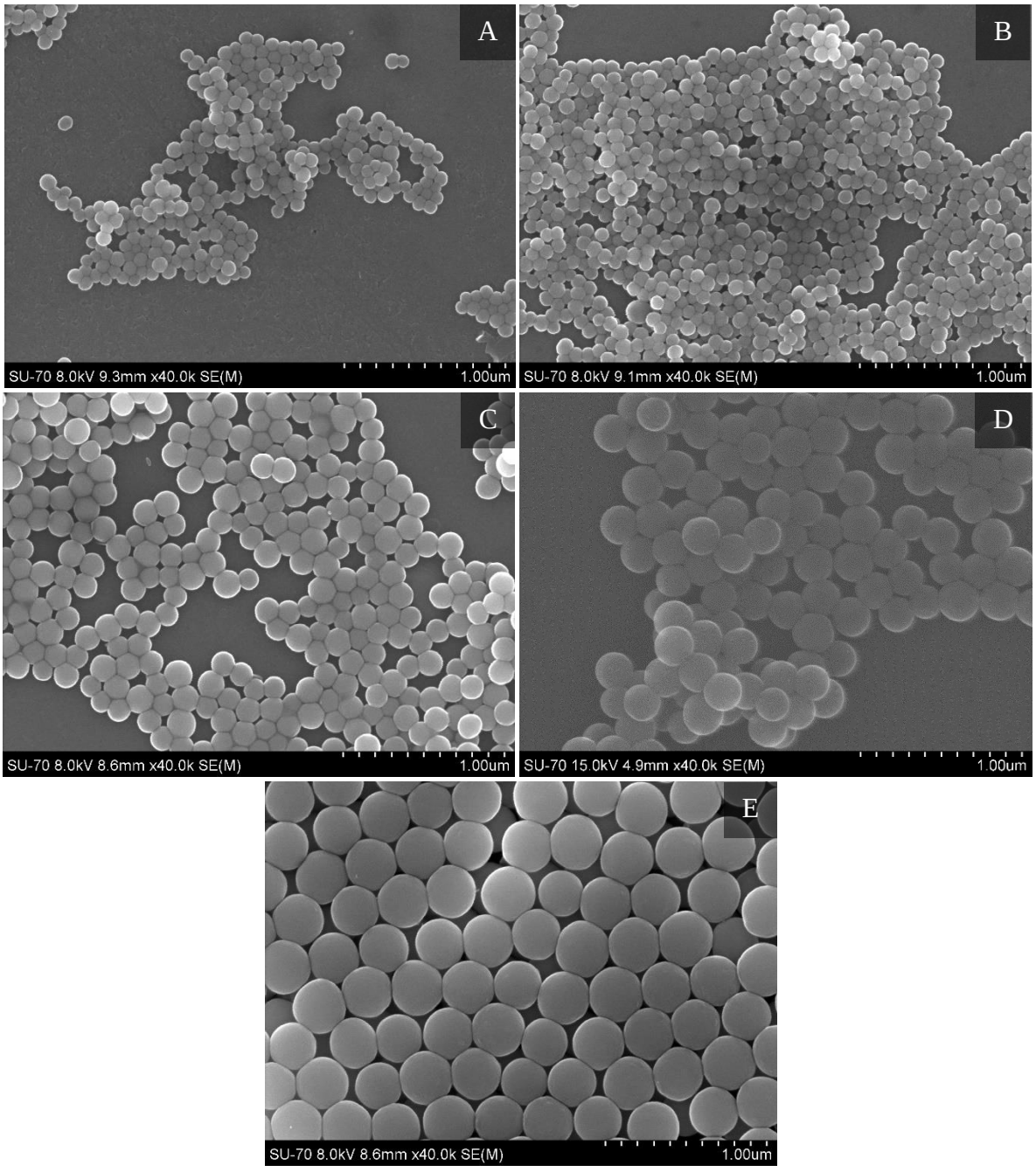

Figure 12 - SEM micrographs of the SiO_2 nanoparticles synthetized through the Stöber method using different ammonia concentrations: A – 0.15 M; B – 0.20 M; C – 0.25 M, D – 0.30 M and E – 0.50 M

The measurement of the particles' diameter carried out based on the SEM micrographs, confirmed that the particles size did in fact increase with increasing ammonia concentrations, as summarized in Table 1. Sample A (synthetized using 0.15 M of ammonia) revealed the smallest particles diameter with 89 ± 8 nm, whereas samples B, C and D (synthetized using 0.20, 0.25 and 0.30 M of ammonia, respectively) showed increasing diameters of 100 ± 12 nm, 155 ± 13 nm and 234 ± 19 nm. Sample E, being the product of the highest ammonia concentration (0.50 M), contained the largest spheres with 321 ± 16 nm in diameter.

The diameter of the obtained particles (samples B, C, D and E) is coherent with the linear dependence of particle diameter with the logarithm of the concentration of NH_4OH in the reaction medium as described by Pinto and co-workers.[109] Although sample A falls outside of the concentration range investigated in the work of Pinto *et al.*, the diameter obtained seems to be in line with other works on synthesis of smaller particles by the Stöber reaction.[115,116]

The determination of the particle's zeta-potential revealed that all the SiO_2 nanoparticles possessed negative surface potential regardless of the size (Table 1). Sample A presented a zeta-potential of -42 ± 2 mV, while samples B and C demonstrated zeta-potential values of -43 ± 3 mV and -38 ± 7 mV, respectively. Samples D and E present values of -31 ± 3 mV and -47 ± 1 mV. This could be justified by the abundance of hydroxyl (-OH) groups on the surface of the particles.[117]

Table 1 - Size and zeta-potential measurements of the different SiO_2 spherical templates obtained through the Stöber reaction

Sample	[NH_3] (M)	Size (nm)	Zeta-potential (mV)
A	0.15	89 ± 8	-42 ± 2
B	0.20	100 ± 12	-43 ± 3
C	0.25	155 ± 13	-38 ± 7
D	0.30	234 ± 19	-31 ± 3
E	0.50	321 ± 16	-47 ± 1

3.1.1 Functionalization of silica templates

The above described abundance of hydroxyl groups on the SiO_2 particles surface allows their functionalization to grant them with a positive surface charge. Adding amino groups to the particles surface through reaction with APTES (Figure 13) will therefore result in particles with marked positive surface charge in 1% (v/v) acetic acid aqueous solutions, forming less aggregates due to the electrostatic repulsion between amino groups, and allowing the deposition of a negatively-charged biopolymer later on.[118]

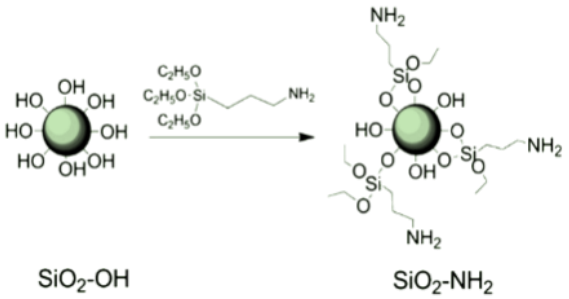

Figure 13 – Schematic representation of the functionalization of SiO_2 templates with amino-groups by reaction with APTES. Adapted from "Formation and characterization of natural polysaccharide hollow nanocapsules via template layer-by-layer self-assembly" - Liu et al.(2012) [110]

Given so, all the samples previously synthetized were subjected to reaction with APTES in ethanol. All the resulting particles maintained their previous integrity, spherical shape and smooth surface, revealing no substantial alterations on their morphology, as depicted by SEM analysis (Figure 14).

The determination of the particles' diameter by analysis on the SEM micrographs showed no relevant changes of the particles' size (Table 2). Sample A_{APTES} revealed a diameter of 89 ± 9 nm, while samples B_{APTES} and C_{APTES} showed diameters of 102 ± 10 nm and 156 ± 13 nm, respectively. Samples D_{APTES} and E_{APTES} presented diameters of 239 ± 11 nm and 326 ± 18 nm, respectively. Overall, one can infer that the particles reaction with APTES does not seem to impact their morphology and size.

The zeta-potential measurements carried out on all samples confirmed the successful functionalization of the SiO_2 particles, expressed by the remarkable inversion of the particles' surface potential when compared to the non-functionalized counterparts (Table 2).

Sample A_{APTES} previous zeta-potential was inverted to 57 ± 1 mV, while sample B_{APTES} revealed a surface charge of 62 ± 5 mV. Samples C_{APTES}, D_{APTES} and E_{APTES} showed potentials of 48 ± 2 mV, 53 ± 2 mV and 86 ± 3 mV, respectively. This alteration of the particle's surface-potential to positive values of more than 40 mV is concordant with the results reported by Liu *et al.*[110]

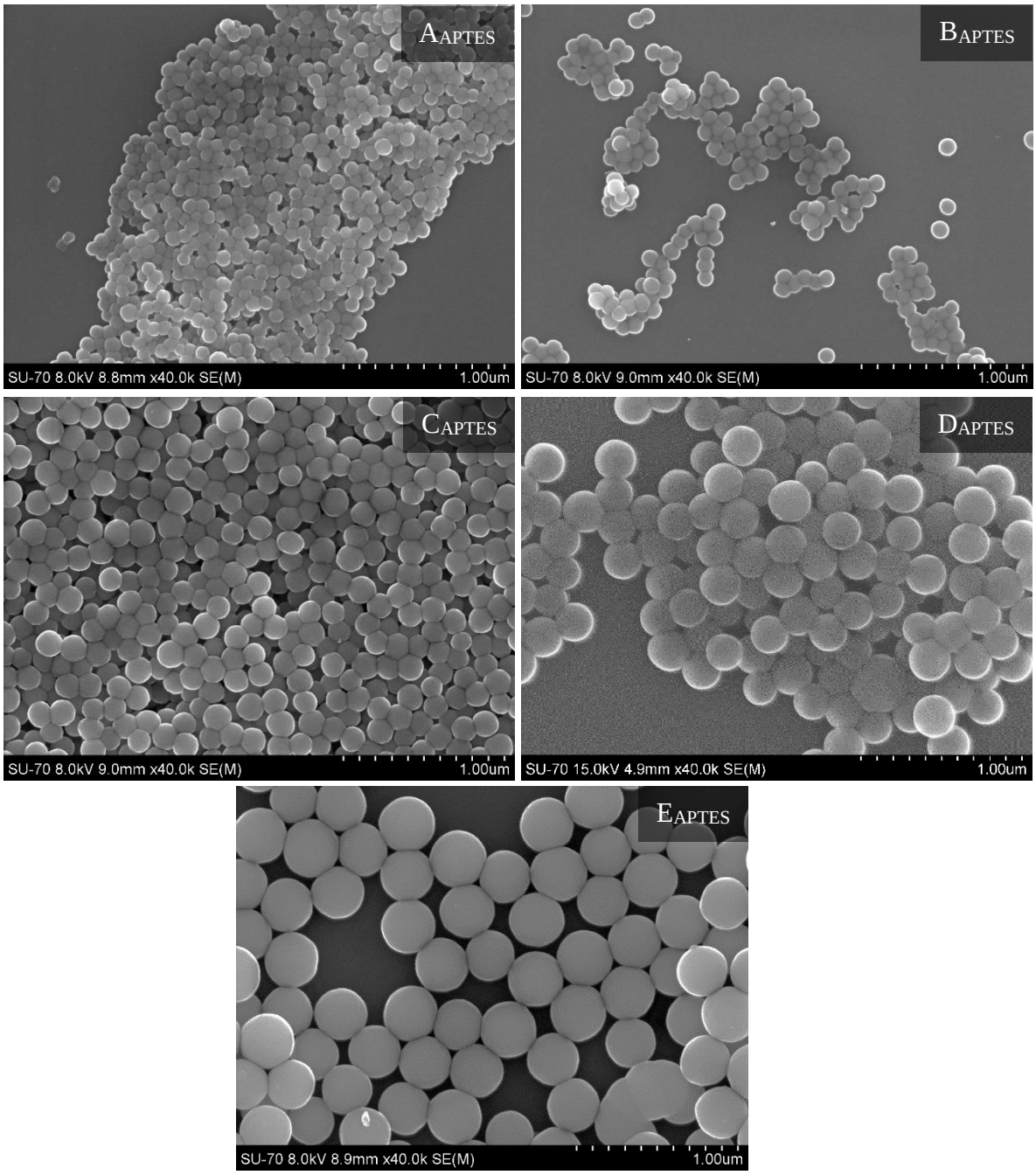

Figure 14 – SEM micrographs of samples A, B, C, D, and E after reaction with APTES for the functionalization with amino-groups

Table 2 - Size and zeta-potential measurements of all SiO_2 samples before and after the functionalization with APTES

	Size (nm)		Zeta-potential (mV)	
Sample	**Si-OH**	**Si-NH_2**	**Si-OH**	**Si-NH_2**
A	89 ± 8	89 ± 9	-42 ± 2	57 ± 1
B	100 ± 12	102 ±10	-43 ± 3	62 ± 5
C	155 ± 13	156 ± 13	-38 ± 7	48 ± 2
D	234 ± 19	239 ± 11	-31 ± 3	53 ± 2
E	321 ± 16	326 ± 18	-47 ± 1	86 ± 3

3.2 Incorporation of model-drug

The assembly of nanocarriers for controlled drug delivery depends on the successful incorporation of the drug in the carrier. In this case, the model-drug (CUR) was previously incorporated into the SiO_2 templates before the deposition of the biopolymers.

In order to understand how the particles size might condition the incorporation of the drug, samples of three different sizes (A_{APTES}, D_{APTES} and E_{APTES}) were all subjected to the same incorporation process. The amount of CUR incorporated in each sample was evaluated by the UV-Vis analysis of the remaining CUR in the medium by the end of the process. The results of this procedure are summarized in Figure 15 and reveal that the percentage of CUR loaded into the templates is higher for smaller particles, decreasing as the particles size increases. Sample A_{CUR} had a total incorporation percentage of 65 ± 5%, while samples D_{CUR} and E_{CUR} showed incorporation percentages of 50 ± 3% and 46 ± 1%, respectively.

The increased surface area of smaller particles, when compared with larger templates, is probably the reason for these incorporation differences. No previous work was found to focus on the analysis of the influence of nanoparticle's size on CUR incorporation. However,

the percentage of CUR incorporation for each sample seems to be similar to the incorporation described in the literature: the work of AbouAitah *et. al.* describes a CUR incorporation of around 70% for particles of approximately 100 nm, while Nasab *et al.* have demonstrated incorporation of 40% for particles with nearly 200 nm and Tiwari *et al.* obtained 50% of CUR incorporation for carriers with around 300 nm (functionalized with APTES and carboxymethyl-cellulose). [119–121]

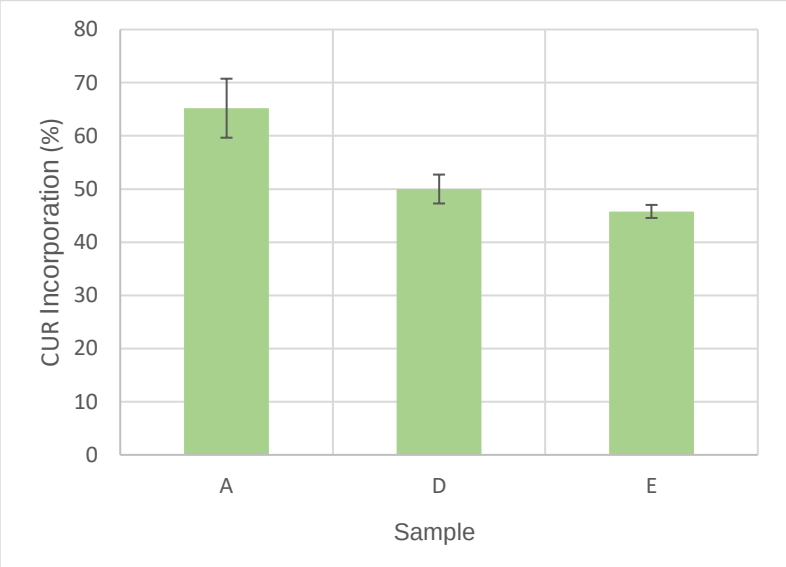

Figure 15 – Graphical representation of the incorporation percentage of curcumin in samples A_{CUR} (89 nm), D_{CUR} (239 nm) and E_{CUR} (326 nm), to evaluate the influence of particle size on incorporation rate.

SEM analysis of the SiO_2 templates after this process (Figure 16) reveals no relevant changes on the particles morphology, integrity and size: sample A_{CUR} showed a diameter of 90 ± 7 nm, while sample D_{CUR} and sample E_{CUR} revealed sizes of 240 ± 17 nm and 327 ± 18 nm, respectively (Table 3).

Surface-charge determination by zeta-potential analysis also revealed no substantial deviations from the functionalized counterparts (Table 3). Sample A_{CUR} kept a zeta-potential of 58 ± 3 mV, while sample D_{CUR} showed a potential of 52 ± 2 mV and sample E_{CUR} of 85 ± 2 mV.

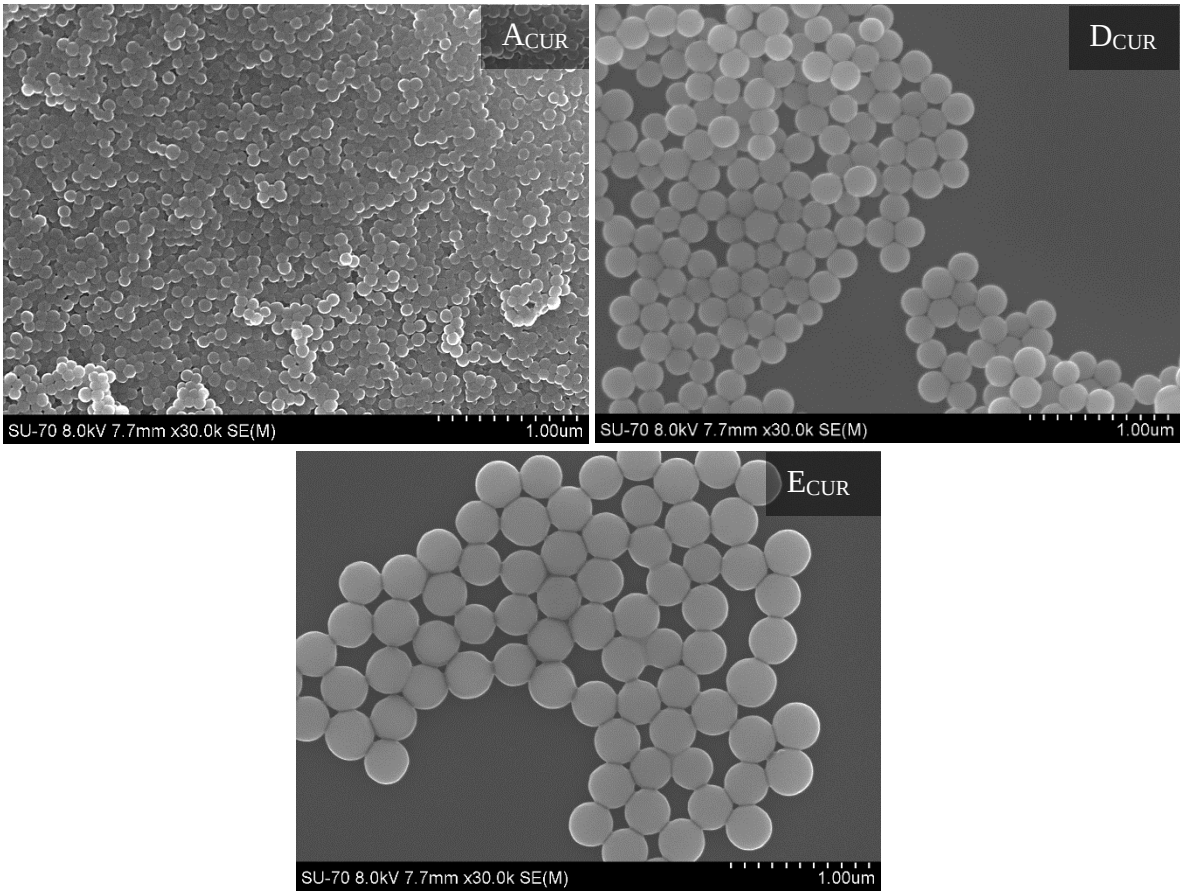

Figure 16 - SEM micrographs of samples A, D and E after CUR incorporation.

Table 3 - Size and zeta-potential measurements of samples A, D and E before and after CUR incorporation

	Size (nm)		Zeta-potential (mV)	
Sample	**Si-NH_2**	**CUR-loaded**	**Si-NH_2**	**CUR-loaded**
A	89 ± 9	90 ± 7	57 ± 1	58 ± 3
D	239 ± 11	240 ± 17	53 ± 2	52 ± 2
E	326 ± 18	327 ± 18	86 ± 3	85 ± 2

3.3 Preparation of lysozyme nanofibrils

LNFs were used as an outer layer for one of the particles later synthetized in this work (refer to 3.4.2). The fibrillation of HEWL was, in this case, induced by the usage of a deep eutectic solvent (DES), namely cholinium chloride : acetic acid (1:1),[113] which was essential to provide the ionic strength of the reactional medium for the fibrillation process. The disruption of the hydrogen-bonds of the native protein originates *β*-dimers that will, under the right conditions, stack and originate nanofibers.

After the fibrillation process, the LNFs suspension was centrifuged to deposit the newly formed nanofibrils. The UV-Vis analysis of the supernatant at 276 nm (the absorption wavelength of aromatic amino acids)[122] allowed the quantification of non-fibrillated lysozyme and the determination of a conversion rate of native HEWL to LNFs of 97.6%, which is coherent with the data reported by Silva *et al.*[113].

In order to verify the nanofibrillar structure of the lysozyme, a sample was treated with thioflavin-T and its fluorescence was measured in a fluorimeter. Thioflavin-T is used as a marker of *β*-sheet structures, since it only exhibits fluorescence when linked to such structures (like protein nanofibrils).[123] In this case, the fluorescence assay revealed a peak at 483 nm, confirming the fluorescence of the sample and indicating the presence of *β*-sheet structures (Figure 17), as discussed elsewhere.[113]

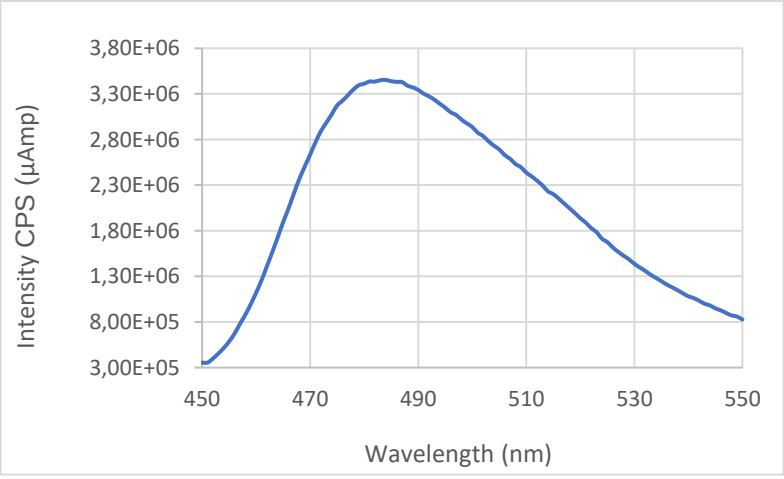

Figure 17 - Fluorescence assay of LNFs suspension marked with thioflavin-T, a marker for the presence of β-sheet structures

STEM visualization of the sample allowed the confirmation of the presence of LNFs on the suspension (Figure 18), where the nanofibers are visibly disperse, individualized and with a length of 545 ± 246 nm and thickness of 20 ± 8 nm. Similar observations were reported by Silva *et al.*[113]. The zeta-potential analysis of the LNFs revealed a potential value of 58 ± 2 mV.

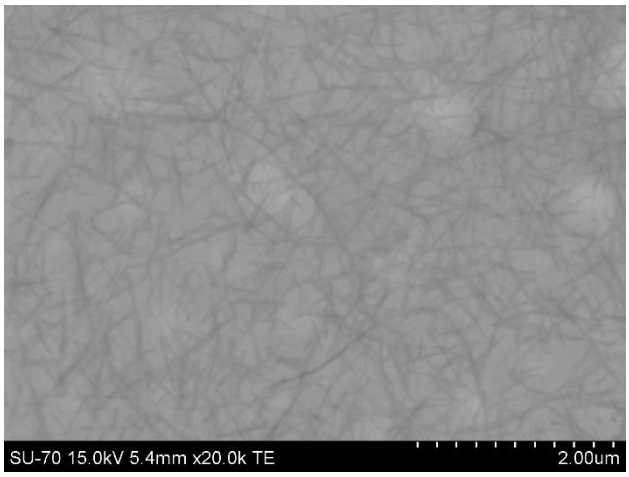

Figure 18 - STEM micrographs of LNFs at 20,000x magnification.

3.4 Preparation of multi-layered systems

The preparation of the multi-layered systems by LbL assembly was carried out using the functionalized SiO_2 template sample D_{CUR} with a diameter of *ca*. 240 nm and zeta-potential of about 53 mV. This sample was selected because of its diameter for two reasons: (i) the technical specificities of working with particles of reduced size are complex, since smaller particles in suspension tend to form aggregates which might compromise the efficient deposition of biopolymers and successful assembly of the individualized spherical carriers, and (ii) the requirements of subsequent biological tests, where larger particles are likely to have a higher impact on the cells' viability, and their internalization by the cells could be jeopardized.

Zeta-potential analysis of the ALG solution confirmed the previously mentioned negative charge of this biopolymer in aqueous solution, with a zeta-value of -40 ± 3 mV.

The same was observed with the CH solution, which revealed a potential of 57 ± 3 mV in 1% acetic acid (v/v) solution.

The successful alternate deposition of polyelectrolytes of opposed charges on the surface of the particles was initially tested in a preliminary assay. This procedure aimed at assessing the feasibility of obtaining nanosystems formed by 5 layers of biopolymers on SiO_2 templates.

3.4.1 Preliminary assay on polyelectrolyte deposition

The LbL process was initialized by the deposition of ALG, the negatively-charged biopolymer, since the particles presented a post-functionalization positive surface charge. The successful coating of the particles with ALG is confirmed by the reversion of the particles surface potential to -35 ± 1 mV. The subsequent deposition of the positively-charged CH revealed similar effects, with the particles surface potential returning to positive values: 42 ± 4 mV. Therefore, the successful deposition of each layer of biopolymer was assessed through the evaluation of the particles surface potential through zeta-potential measurements. The results, summarized in Figure 19, demonstrate that the zeta-potential drastically shifted after every layer deposition, leading to the conclusion that every layer was successfully deposited on the particles surface.

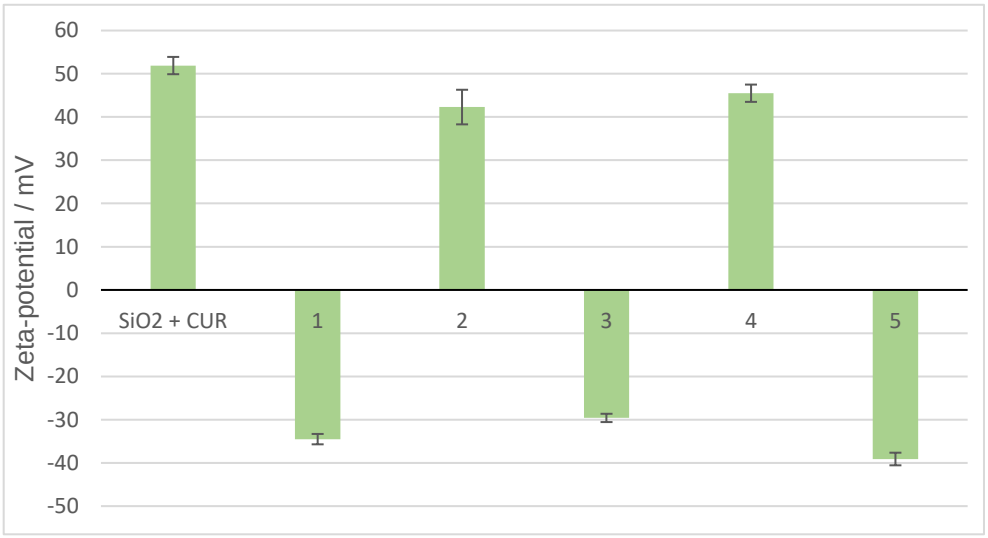

Figure 19 – Particles surface potential after each layer deposition. SiO_2+CUR represents the CUR incorporated templates, while the numbers (1-5) represent the number of biopolymer layers deposited: 1 (ALG), 2 (ALG/CH), 3 (ALG/CH/ALG), 4 (ALG/CH/ALG/CH) and 5 (ALG/CH/ALG/CH/ALG).

SEM visualization of the sample revealed that after the deposition of the five biopolymeric layers (ALG, CH, ALG, CH, ALG), the particles maintain their spherical shape, individuality and integrity, as illustrated in Figure 20.

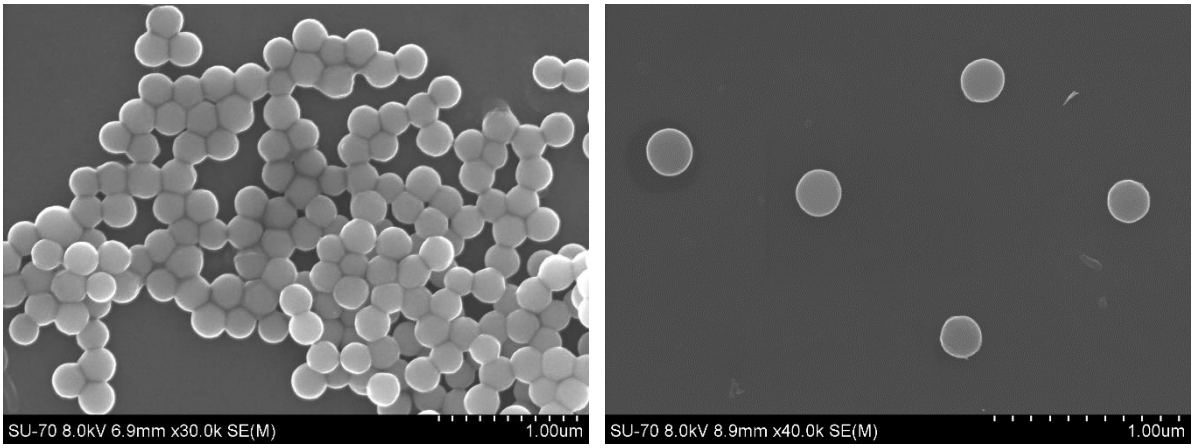

Figure 20 - SEM micrographs of the sample after the deposition of the 5 biopolymeric layers

However, size evaluation seemed to reveal an increase on the particles' diameter after the deposition of the five layers of biopolymers. The diameter of the particles after deposition was 257 ± 13 nm, which might indicate a slight increment of size when compared to the post-incorporated templates (Table 4). This possible increase on the particles' diameter, together with the reversion of the potential, is another indicator of a successful deposition of the five layers of biopolymers on the surface of the functionalized spherical templates loaded with CUR.

Table 4 – Size and zeta-potential of the CUR-loaded templates and the 5-layered nanosystems, all obtained from sample D.

	Size (nm)		Zeta-potential (mV)	
Sample	**CUR-loaded templates**	**5-layered systems**	**CUR-loaded templates**	**5-layered systems**
D	240 ± 17	257 ± 13	52 ± 2	-50 ± 1

Altogether, the results from this preliminary assay demonstrate that the successful deposition of multiple biopolymeric layers is possible through LbL assembly on SiO_2 nanoparticles of the described size, allowing the control of the final nanosystems diameter, and resulting in disperse and individualized sphere-shaped nanoparticles.

3.4.2 Preparation of ALG/CH and ALG/LNFs particles

In order to explore the potential effect of protein nanofibrils as building blocks for nanosystems obtained through LbL assembly, two distinct types of two-layered particles were then manufactured, namely ALG/CH and ALG/LNFs covered SiO_2 templates.

The deposition of the first layer, ALG, on all templates was achieved as earlier described (refer to section 2.5), and confirmed by the reversal of the particle's zeta-potential to negative values of -22 ± 1 mV (Figure 21). The resulting particles were then divided into two different batches and either CH or LNFs were deposited as the outer layer.

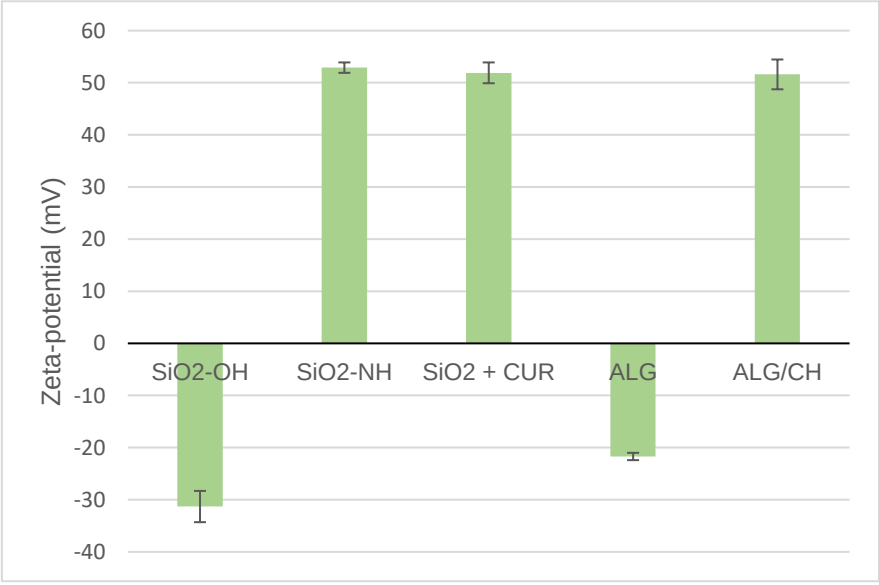

Figure 21 - Particles surface potential after functionalization, incorporation of CUR and deposition of each biopolymeric layer (ALG and CH).

Regarding the ALG/CH particles, the zeta-potential analysis of the surface potential confirmed the successful deposition of CH (Figure 21 and Table 5), with 52 ± 3 mV. SEM observation of the resulting systems showed the expected spherical particles (Figure 22). The particles, although well-individualized and disperse, seem to show a slight alteration of the surface smoothness when observed at higher magnification, possibly due to the two layers of deposited biopolymer.

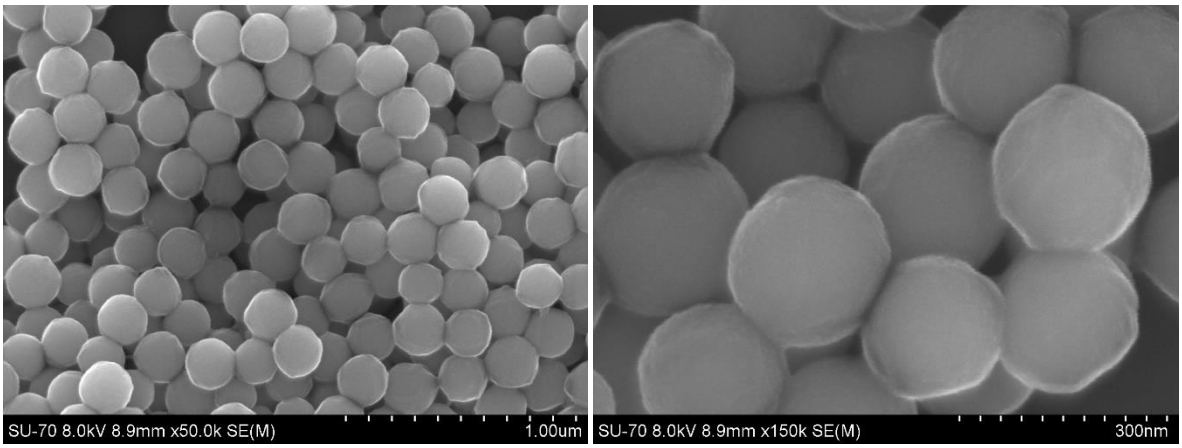

Figure 22 - SEM micrographs of the ALG/CH particles. At higher magnification, the particles reveal a mild modification of their surface (when compared with bare templates).

Analysis of ALG/CH particles' diameter seemed to reveal a slight increase on the particles size to 243 ± 8 nm caused by the deposition of ALG and CH (Table 5).

Table 5 - Size and zeta-potential of the CUR-loaded templates and the ALG/CH layered particles.

	Size (nm)		Zeta-potential (mV)	
Sample	**CUR-loaded templates**	**ALG/CH**	**CUR-loaded templates**	**ALG/CH**
D	240 ± 17	243 ± 8	52 ± 2	52 ± 3

Similarly, particles with LNFs as the outer layer (ALG/LNFs) also demonstrated a reversion on the zeta-potential value, with 29 ± 1 mV as surface charge (Figure 23). One can, therefore, infer that the deposition of the LNFs on the particles was also effective.

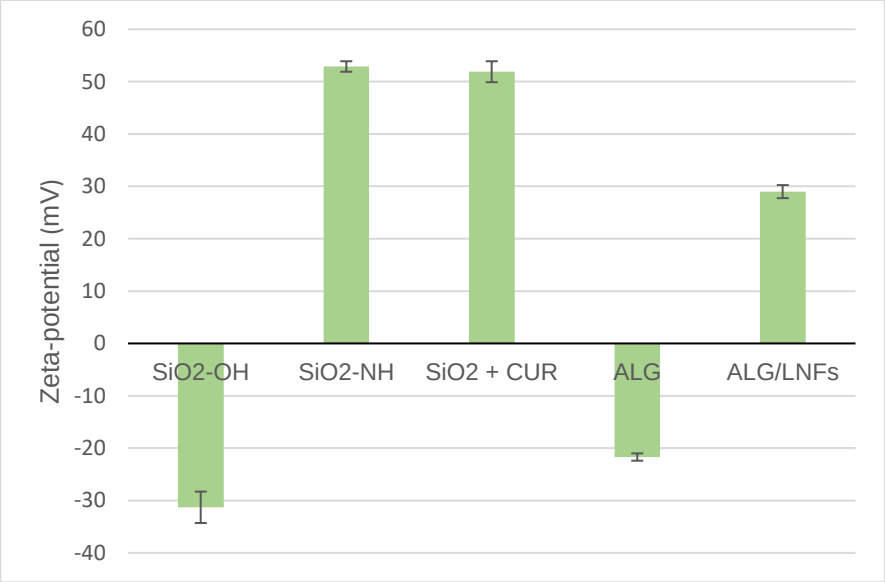

Figure 23 - Particles surface potential after functionalization, incorporation of CUR and deposition of each biopolymeric layer (ALG and LNFs).

The SEM observation of the ALG/LNFs nanoparticles showed that the resulting particles were still individualized, disperse and spherical (Figure 24). However (and oppositely to what happens with ALG/CH), when seen at higher magnifications, the particles seem covered by structures of fibrillar shape. The analysis of the particles' diameter was, once more, coherent with the deposition of both biopolymers, showing a possible slight increase in size from 240 to 242 ± 8 nm (Table 6).

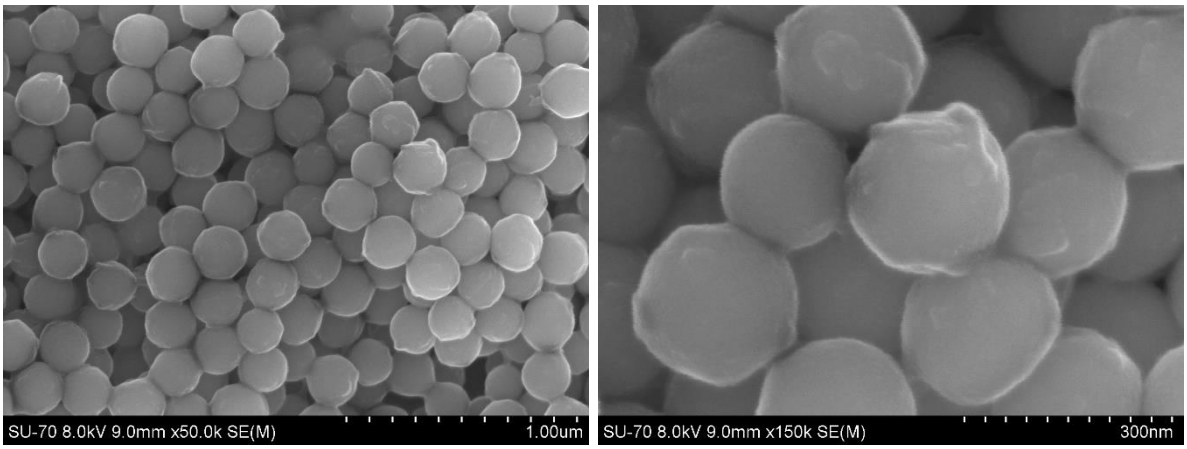

Figure 24 – SEM micrographs of ALG/LNFs particles. At higher magnification, the particles reveal structures of fibrillar shape at their surface.

Table 6 - Size and zeta-potential comparison between CUR-loaded templates and the ALG/LNFs layered particles.

	Size (nm)		Zeta-potential (mV)	
Sample	**CUR-loaded templates**	**ALG/LNFs**	**CUR-loaded templates**	**ALG/LNFs**
D	240 ± 17	242 ± 8	52 ± 2	29 ± 1

3.5 Drug release assay

The goal of the nanocarriers described in this study is to be able to release the model-drug, CUR, in a controlled and sustained way. To evaluate this, the particles (i) ALG/LNFs, (ii) ALG/CH and (iii) CUR-loaded templates (SiO_2 + CUR) were dispersed in a PBS solution and left under moderate stirring for a 24 hours period. Aliquots of the media were taken at predefined time-points and the concentration of CUR assessed by UV-vis spectroscopy. PBS was selected for this study due to its close resemblance to the pH, osmolarity and ion concentration of biological fluids, providing valuable and transposable data about the probable behaviour of the nanocarriers in a biological context.

The results of the drug release assay are summarized in Figure 25. A clear burst release is observable on the first 2 hours of the experiment for all samples, after which the cumulative release remains relatively constant for 24 hours. CUR-loaded templates without biopolymeric layers have a higher release of CUR along the assay, *i.e.* 46%. On the other hand, the two-layered counterparts show lower release of the model-drug: ALG/CH particles released 28% of the incorporated CUR, while ALG/LNFs nanosystems released only 23% after 24 hours.

These data show that the existence of biopolymeric layers coating the CUR-loaded templates causes a notorious diminishing of the release of the drug to the PBS medium, which is concordant with the results of multiple works in the area.[e.g.111,124] The difference between the release from ALG/CH and ALG/LNFs particles might be an indicator that the presence of LNFs as the outer layer promotes a lesser release of CUR, eventually by constituting an improved obstacle to CUR's diffusion from the particle – forcing the drug to go through a more tortuous path to be released.

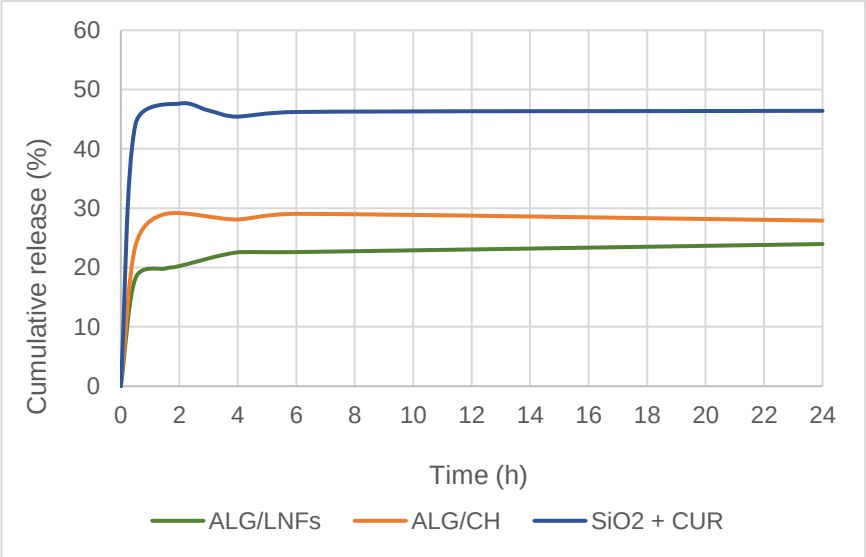

Figure 25 – Cumulative release (%) of CUR from uncoated templates (SiO_2 + CUR) and two-layered nanosystems (ALG/LNFs and ALG/CH) for 24 hours.

3.6 *In vitro* cytotoxicity assays

The cytotoxicity potential of the previously developed materials was evaluated by the MTT assay towards the human liver cancer HepG2 cell line with described sensitivity to CUR[125,126] and included in several works for the assessment of nanoparticles biological activity.[127–129] The MTT essay relies on the conversion of MTT into a purple coloured formazan by viable cells (Figure 26). The quantity of formazan (measured by the sample's absorbance at 570 nm) is used to infer quantity of viable cells, since dead cells are unable to reduce MTT into this metabolite.

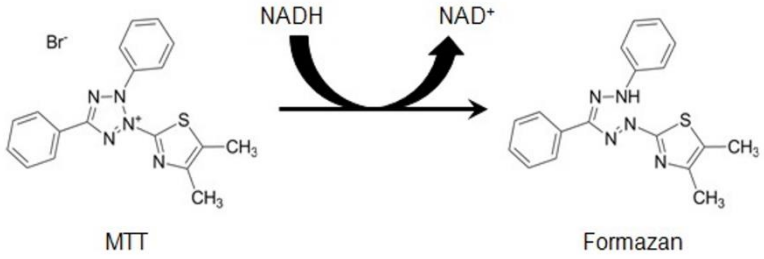

Figure 26 - Reduction of MTT into formazan by viable cells. Reproduced from "Cell viability assays" Riss et al (2014) [132]

Herein, cells were exposed to four different samples, namely the blank SiO_2 templates, SiO_2 loaded with CUR (SiO_2+CUR), and the bi-layered systems (ALG/CH or ALG/LNFs) containing CUR. Two different exposure periods were tested, *viz*. 24 and 48 hours, for the five sample concentrations of 12.5, 25, 50, 100 and 200 $\mu g.mL^{-1}$.

The results for the 24-hours MTT assay, presented in Figure 27, show that the bare SiO_2 templates (without CUR) are non-cytotoxic up to concentrations of 100 $\mu g.mL^{-1}$ but are already considered cytotoxic at a concentration of 200 $\mu g.mL^{-1}$, with a cell viability slightly below the 70% threshold.[114] Thus, one can easily infer that, at such a high concentration, the bare SiO_2 templates prove to be cytotoxic for HepG2 cells. In fact, all particles reveal cytotoxic potential at 200 $\mu g.mL^{-1}$, presumably derived from their abundance in the medium affecting the normal cell growth and proliferation (and not exclusively due to their characteristics).[130]

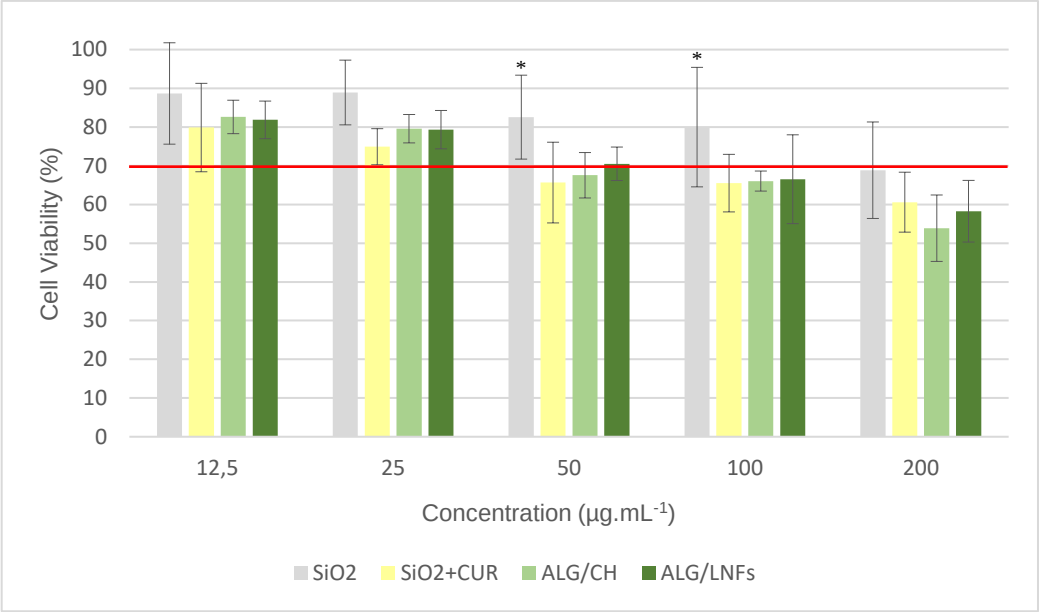

Figure 27 - Results of cell viability from the 24-hour MTT assay. The line in red, at 70% viability, represents the cytotoxic threshold below which one will consider the cytotoxic effect to be relevant. An asterisk (*) marks the statistically different results

On the other hand, CUR-loaded templates are non-cytotoxic only up to concentrations of 25 µg.mL^{-1}. At 50 µg.mL^{-1}, they begin to demonstrate notorious cytotoxic effect (reducing the percentage of viable cells to 66%). At the same concentration, bare SiO_2 templates (without CUR) have a reduced effect on cell viability (83% of the cells are still viable by the end of the study). The statistical analysis of the data confirms the significant difference between these effects (*p-value* = 0.001).

When exposed to 100 µg.mL^{-1} of CUR-loaded templates, only 65% of the cells remained viable. At this concentration, bare SiO_2 templates showed no relevant cytotoxic potential (with 79% cell viability). Once more, this difference is statistically significative (*p-value* = 0.0092).

This notorious contrast, coherently observed at both concentrations, is in line with the assumption that the presence of CUR on the particles grants them a cytotoxic effect against HepG2 cells, as already discussed.

Regarding both the two-layered systems, ALG/CH and ALG/LNFs, their cytotoxic effect is only noteworthy at 50 µg.mL^{-1}, when cell viability reaches values of 68% and 71%, respectively. However, when compared with the unlayered CUR-loaded counterparts, the

statistical analysis of the data confirms the absence of significant differences. Similar conclusions can be drawn from the results obtained at a concentration of 100 µg.mL^{-1} : the effects of CUR-loaded templates, ALG/CH and ALG/LNFs particles remain quite similar (65, 66 and 67% of cell viability, respectively), with no significant statistical differences.

Considering the sustained release profile of CUR obtained in the previous section (refer to 3.5), one could expect the similar cytotoxic effect observed between the two-layered systems. Yet, the results of the comparison of those with the unlayered counterparts might indicate that the drug-release profile previously tested is not a direct cause for the cytotoxic effect *per se* – ALG/CH and ALG/LNFs, even though demonstrating lower release of CUR after 24 hours, have achieved the same cytotoxicity results of the un-layered counterparts. This could be an indication that the biopolymeric layers do not compromise the cytotoxic effect of the particles, and that these carriers still release enough CUR to impact the cells viability – possibly by being internalized and/or having their polysaccharides degraded, with consequent release of CUR.[131]

Given the results obtained for the 24-hour assay, the 48-hour MTT assay was carried out solely on concentrations of 25, 50 and 100 µg.mL^{-1} of each particle. The results are shown in Figure 28.

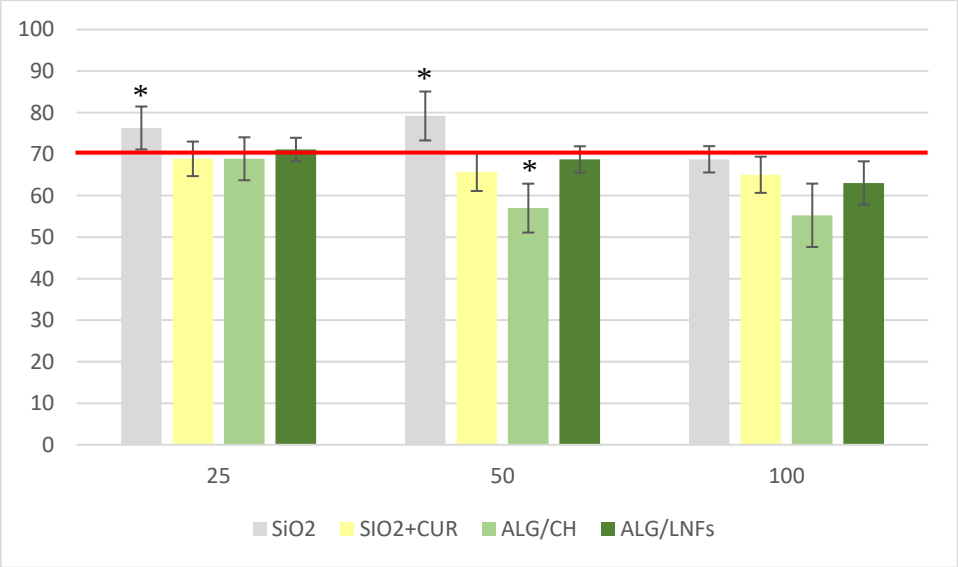

Figure 28 – Results of cell viability from the 48-hour MTT assay. The line in red, at 70% viability, represents the cytotoxic threshold below which one will consider relevant cytotoxic effect. An asterisk (*) marks the statistically different results

After an exposure of 48 hours to the particles, the bare SiO_2 templates reveal cytotoxic potential at 100 $\mu g.mL^{-1}$ concentration – similarly to what happens to all the other samples tested.

Nevertheless, at 50 $\mu g.mL^{-1}$, the results are coherent with the ones obtained previously: CUR-loaded templates show, once more, a higher cytotoxic potential (66%) than the drug-free counterparts (79%). This difference is statistically significant (*p-value* = 0.0001). At this concentration, ALG/LNFs particles still have very similar effects to the SiO_2+CUR (revealing 69% of the cells are still viable by the end of the assay), with no statistically significant differences. Yet, ALG/CH particles, with 57% of cell viability, prove to cause significantly more impact than SiO_2+CUR (*p-value* = 0.0362) and ALG/LNFs (*p-value* = 0.0053). This is a sign that, somehow, ALG/CH particles have a higher impact on cell viability than every other particle tested, after the 48-hour exposure.

At the concentration of 25 $\mu g.mL^{-1}$, statistically significant differences (*p-value* = 0.0033) can only be found between the drug-free templates (with 76% cell viability) and the CUR-loaded silica (with 69%). The layered particles and the CUR-loaded templates have similar effect on the cells, with ALG/CH particles with 69% viability and ALG/LNFs with 71%.

The thorough analysis of the cytotoxic effect of ALG/CH and ALG/LNFs' coated particles would still depend on the realization of the same MTT assay for nanocarriers without the drug (yet still containing the layers of biopolymers), in order to indubitably rule out an eventual cytotoxic effect derived from the components of the carrier itself (either ALG, CH or LNFs). However, and due to the limited amount of time left by the end of this work, the synthesis, characterization and testing of such nanoparticles was not viable.

4 Conclusions and future work

The aim of this work was the preparation and characterization of nanocarriers for the controlled release of anticancer drugs: specifically, the construction of nanoparticles from CH, ALG and LNFs through LbL assembly on SiO_2 templates loaded with a model-drug, namely curcumin. To achieve this, SiO_2 templates were first synthetized through the Stöber method. Well-defined and disperse spheres of five different sizes were obtained by using five different concentrations of ammonia in the reaction: sample A (89 ± 8 nm), sample B (100 ± 12 nm), sample C (155 ± 13 nm), sample D (234 ± 19 nm) and sample E (321 ± 16 nm). Analysis of the zeta-potential revealed that all these particles were negatively-charged.

Subsequent functionalization by reaction with APTES was assessed by the reversion of the spheres surface charge to positive values, with sample A (with a previous zeta-potential of -42 ± 2 mV) showing a potential of 57 ± 1 mV, while samples B and C (previously with zeta-potential values of -43 ± 3 mV and -38 ± 7 mV) inverted their surface charge to 62 ± 5 mV and 48 ± 2 mV, respectively. Samples D and E analysis of the surface charge presents values of 53 ± 2 mV and 86 ± 3 mV (a clear inversion of the previous measurements of -31 ± 3 mV and -47 ± 1 mV). SEM observation of the templates revealed no relevant alteration of the morphological or dimensional characteristics of the spheres: sample A diameter post-functionalization was kept at 89 ± 9 nm, while samples B, C and D showed diameters of 102 ± 10 nm, 156 ± 13 nm and 239 ± 11 nm, respectively. Sample E also had no notorious size changes, keeping a diameter of 326 ± 18 nm.

The incorporation of CUR, the model-drug used in this study, was carried out on samples A, D and E to understand the role of particle size on incorporation rate. The results demonstrated that smaller templates show higher incorporation percentage, *i.e.* sample A incorporated 65 ± 5% of the total CUR, while samples D and E presented incorporation

percentages of 50 ± 3% and 46 ± 1%, respectively. The incorporation process did not seem to affect the templates' size nor their surface charge.

Multi-layered systems were prepared through the alternate deposition of ALG and CH on the functionalized CUR-loaded SiO_2 spheres, specifically sample D. The systematic reversion of the particles' surface potential after each deposition of a polysaccharide confirmed the successful coating of the nanoparticles with every layer of biopolymer. SEM observation confirmed that the resulting nanoparticles still possessed the spherical shape and individuality after the five depositions of CH and ALG of the preliminary test.

LNFs were successfully prepared by using a DES as fibrillation agent of HEWL. Conversion rate of native protein into LNFs was 97.6%, and the nanofibrillar shape of LNFs was confirmed by the peak of fluorescence at 480 nm in a thioflavin-T fluorescence assay. Posterior STEM analysis of the LNFs suspension confirmed the presence of individual and disperse nanofibrils of 545 ± 246 nm in length, and a thickness of 20 ± 8 nm, while zeta-potential measurements revealed the LNFs to be positively-charged (58 ± 2 mV).

Two-layered particles were also obtained by depositing either ALG/CH or ALG/LNFs on sample D. Once more, the constant reversal of the zeta-potential and SEM observation of such particles confirmed the successful assembly by the LbL technique. The two-layered particles were posteriorly subjected to a drug release assay in PBS, which showed that bare CUR-loaded templates have a significantly higher release of CUR (46%) than their two-layered counterparts (ALG/CH particles released 28%, while ALG/LNFs nanosystems released only 23% of the incorporated CUR). Therefore, one can conclude that the biopolymeric layers coating the CUR-loaded templates allowed a sustained release of the drug to the medium, and that using LNFs as the outer layer might promote a reduced release of CUR.

Biological impact of the produced carriers was investigated through MTT assays that verified the cytotoxic effect of CUR on HepG2 cells (with bare CUR-loaded templates consistently presenting a significantly higher cytotoxic effect). These assays also demonstrated a similar cytotoxic effect between the ALG/LNFs and ALG/CH and against the un-layered CUR-loaded templates (around 30% of cell death), proving that the existence of two polymeric layers on the particles, although affecting CUR release, does not

compromise the cytotoxic effect of the CUR-loaded nanocarriers against HepG2 cells. In the future, the testing of particles with a higher number of layers could also be performed in order to enlighten if this cytotoxic effect is modified by the amount of biopolymeric coatings on the particles.

Some other future approaches to this work could include, for instance, the removal of the SiO_2 template, creating hollow capsules exclusively containing the drug to be released. Tests with other drugs could also provide relevant new data about the behaviour of these nanocarriers as controlled release agents. The cytotoxic evaluation of ALG/CH and ALG/LNFs nanoparticles without CUR could also aid in a better understanding of the cytotoxicity of the systems by themselves, without the incorporated model-drug.

The inclusion of a targeting molecule or a fluorescent marker at the particles' surface could also represent a relevant addition to this study, providing new information about the nanocarriers behaviour and eventually improving their effect on cancer cells.

A detailed characterization of these nanosystems behaviour and impact on tumour and normal cells (specifically their effect on the cell cycle and apoptosis) should also be performed in order to fully understand their potential for eventual therapeutic applications.

5 References

1. Geneva: World Health Organization; Status of the health-related SDGs. in *World health statistics 2017: monitoring health for the SDGs, Sustainable Development Goals* 29–35 (2017). doi:ISBN 978-92-4-156548-6
2. World Health Organization. WHO | Cancer - Key Statistics. Available at: http://www.who.int/cancer/resources/keyfacts/en/. (Accessed: 24th January 2018)
3. Siegel, R. L., Miller, K. D. & Jemal, A. Cancer statistics, 2018. *CA. Cancer J. Clin.* **68,** 7–30 (2018).
4. Siegel, R. L., Miller, K. D. & Jemal, A. Cancer statistics, 2017. *CA. Cancer J. Clin.* **67,** 7–30 (2017).
5. Miller, K. D. *et al.* Cancer treatment and survivorship statistics, 2016. *CA. Cancer J. Clin.* **66,** 271–289 (2016).
6. WHO. Cancer Country Profiles: Portugal. 2 (2014). Available at: https://www.who.int/cancer/country-profiles/en/. (Accessed: 21st January 2018)
7. National Cancer Institute. What Is Cancer? Available at: https://www.cancer.gov/about-cancer/understanding/what-is-cancer. (Accessed: 24th January 2018)
8. Hanahan, D. & Weinberg, R. A. Hallmarks of cancer: The next generation. *Cell* **144,** 646–674 (2011).
9. Knudson, A. G. Two genetic hits (more or less) to cancer. *Nat. Rev. Cancer* **1,** 157–162 (2001).
10. Surget, S. & Bourdon, J. Uncovering the role of p53 splice variants in human malignancy : a clinical perspective. *Onco. Targets. Ther.* 57–68 (2014).
11. Balmain, A. Cancer genetics : from Boveri and Mendel to microarrays. *Nat. Rev. Cancer* **1,** 79–82 (2001).
12. Whiteman, D. C. & Wilson, L. F. The fractions of cancer attributable to modifiable factors : A global review. *Cancer Epidemiol.* **44,** 203–221 (2016).
13. Schottenfeld, D. & Mph, J. B. The cancer burden attributable to biologic agents. *Ann. Epidemiol.* **25,** 183–187 (2015).
14. Yancopoulos, G. D. *et al.* Vascular-specific growth factors and blood vessel formation. *Nature* **407,** 242–248 (2000).
15. Carmeliet, P. & Jain, R. K. Angiogenesis in cancer and other diseases. *Nature* 249–257 (2000).
16. Talmadge, J. E. & Fidler, I. J. AACR Centennial Series : The Biology of Cancer Metastasis : Historical Perspective. *Am. Assoc. Cancer Res. J.* **70,** 5649–5670 (2010).

17. Wyld, L., Audisio, R. A. & Poston, G. J. The evolution of cancer surgery and future perspectives. *Nat. Rev. Clin. Oncol.* **12,** 1–10 (2015).

18. National Breat Cancer Foundation, Inc. Available at: http://www.nationalbreastcancer.org/. (Accessed: 25th January 2018)

19. Baskar, R., Lee, K. A., Yeo, R. & Yeoh, K. Cancer and Radiation Therapy : Current Advances and Future Directions. *Int. J. Med. Sci.* **9,** 193–199 (2012).

20. Kim, B. M. *et al.* Therapeutic Implications for Overcoming Radiation Resistance in Cancer Therapy. *Int. J. Mol. Sci.* **16,** 26880–26913 (2015).

21. Helmy, K. Y. & Nahas, G. R. Cancer immunotherapy : accomplishments to date and future promise. *Ther. Deliv.* **4,** 1307–1320 (2013).

22. Alatrash, G., Jakher, H., Stafford, P. D. & Mittendorf, E. A. Cancer immunotherapies , their safety and toxicity. *Expert Opin. Drug Saf.* 1–15 (2013).

23. Alldredge, B. K. *et al. Koda-Kimble and Young's applied therapeutics: The clinical use of drugs*. *Koda-Kimble and Young's Applied Therapeutics: The Clinical Use of Drugs* (2013).

24. Elder, K., Dixon, J. M., Blackmur, J. P. & Laurie, J. Endocrine therapy for cancer. *Surg. - Oxford Int. Ed.* **36,** 128–133 (2018).

25. Lind, M. J. Principles of cytotoxic chemotherapy. *Medicine (Baltimore).* **36,** 19–23 (2007).

26. Kalyanaraman, B. Teaching the basics of cancer metabolism: Developing antitumor strategies by exploiting the differences between normal and cancer cell metabolism. *Redox Biol.* **12,** 833–842 (2017).

27. Gurney, H. How to calculate the dose of chemotherapy. *Br. J. Cancer* **86,** 1297–1302 (2002).

28. Friberg, S. & Nyström, A. M. Nanotechnology in the war against cancer: new arms against an old enemy - a clinical view. *Future Oncol.* **11,** 1961–75 (2015).

29. Wicki, A., Witzigmann, D., Balasubramanian, V. & Huwyler, J. Nanomedicine in cancer therapy: Challenges, opportunities, and clinical applications. *J. Control. Release* **200,** 138–157 (2015).

30. Kittitheeranun, P. *et al.* Layer-by-layer engineered nanocapsules of curcumin with improved cell activity. *Int. J. Pharm.* **492,** 92–102 (2015).

31. Chen, J. *et al.* Theranostic Multilayer Capsules for Ultrasound Imaging and Guided Drug Delivery. *ACS Nano* **11,** 3135–3146 (2017).

32. Hammond, P. T. Building biomedical materials layer-by-layer. *Mater. Today* **15,** 196–206 (2012).

33. Vilela, C., Figueiredo, A. R. P., Silvestre, A. J. D. & Freire, C. S. R. Multilayered materials based on biopolymers as drug delivery systems. *Expert Opin. Drug Deliv.* **14,** 189–200 (2017).

34. Gopi, S. & Amalraj, A. Effective Drug Delivery System of Biopolymers Based On Nanomaterials and Hydrogels - A Review. *Drug Des. Open Access* **5,** (2016).

35. Alvarez-Lorenzo, C., Blanco-Fernandez, B., Puga, A. M. & Concheiro, A. Crosslinked ionic polysaccharides for stimuli-sensitive drug delivery. *Adv. Drug Deliv. Rev.* **65,** 1148–1171 (2013).

36. Foroughi, J., Mirabedini, A. & Warren, H. Hydrogels Fibers. in *Hydrogels* 75–105 (2018). doi:10.1007/978-1-4614-0881-9_4

37. Nsor-Atindana, J. *et al.* Functionality and nutritional aspects of microcrystalline cellulose in

food. *Carbohydr. Polym.* **172,** 159–174 (2017).

38. Delattre, C., Laroche, C. & Michaud, P. Production of bacterial and fungal polysaccharides. in *Advances in Fermentation* 483–522 (2007).

39. Society, A. C. Hyaluronic acid. (2018). Available at: https://www.acs.org/content/acs/en/molecule-of-the-week/archive/h/hyaluronic-acid.html?cid=home_motw. (Accessed: 12th December 2018)

40. Varun, T. K. *et al.* Extraction of chitosan and its oligomers from shrimp shell waste, their characterization and antimicrobial effect. *Vet. World* **10,** 170–175 (2017).

41. Kean, T. & Thanou, M. Biodegradation, biodistribution and toxicity of chitosan. *Adv. Drug Deliv. Rev.* **62,** 3–11 (2010).

42. Bernkop-Schnürch, A. & Dünnhaupt, S. Chitosan-based drug delivery systems. *Eur. J. Pharm. Biopharm.* **81,** 463–469 (2012).

43. K. Y. Lee, D. J. M. Alginate : properties and biomedical applications. *Prog. Polym. Sci.* **37,** 106–126 (2012).

44. Grant, G. T., Morris, E. R., Rees, D. A., Smith, P. J. C. & Thom, D. Biological interactions between polysaccharides and divalent cations: The egg-box model. *FEBS Lett.* **32,** 195–198 (1973).

45. Gombotz, W. R. & Wee, S. Protein release from alginate matrixes. *Adv. Drug Deliv. Rev.* **31,** 267–285 (1998).

46. Chickering, D. E. & Mathiowitz, E. Bioadhesive microspheres: I. A novel electrobalance-based method to study adhesive interactions between individual microspheres and intestinal mucosa. *J. Control. Release* **34,** 251–262 (1995).

47. Sun, G. *et al.* Dextran hydrogel scaffolds enhance angiogenic responses and promote complete skin regeneration during burn wound healing. *Proc. Natl. Acad. Sci.* **108,** 20976–20981 (2011).

48. Banerjee, A. & Bandopadhyay, R. Use of dextran nanoparticle: A paradigm shift in bacterial exopolysaccharide based biomedical applications. *Int. J. Biol. Macromol.* **87,** 295–301 (2016).

49. Dosio, F., Arpicco, S., Stella, B. & Fattal, E. Hyaluronic acid for anticancer drug and nucleic acid delivery. *Adv. Drug Deliv. Rev.* **97,** 204–236 (2016).

50. Rivkin, I. *et al.* Paclitaxel-clusters coated with hyaluronan as selective tumor-targeted nanovectors. *Biomaterials* **31,** 7106–7114 (2010).

51. Han, S. E. *et al.* Cationic derivatives of biocompatible hyaluronic acids for delivery of siRNA and antisense oligonucleotides. *J. Drug Target.* **17,** 123–132 (2009).

52. Abeer, M. M., Mohd Amin, M. C. I. & Martin, C. A review of bacterial cellulose-based drug delivery systems: Their biochemistry, current approaches and future prospects. *J. Pharm. Pharmacol.* **66,** 1047–1061 (2014).

53. Elzoghby, A. O., Samy, W. M. & Elgindy, N. A. Protein-based nanocarriers as promising drug and gene delivery systems. *J. Control. Release* **161,** 38–49 (2012).

54. Dadparvar, M. *et al.* HI 6 human serum albumin nanoparticles-Development and transport over an in vitro blood-brain barrier model. *Toxicol. Lett.* **206,** 60–66 (2011).

55. Elzoghby, A. O., Samy, W. M. & Elgindy, N. A. Albumin-based nanoparticles as potential controlled release drug delivery systems. *J. Control. Release* **157,** 168–182 (2012).

56. Elblbesy, M. A. Hemocompatibility of Albumin Nanoparticles as a Drug Delivery System—An <i>in Vitro</i> Study. *J. Biomater. Nanobiotechnol.* **07,** 64–71 (2016).

57. Jahanshahi, M. & Najafpour, G. D. Production of biological nanoparticles from bovine serum albumin for drug delivery. *African J. Biotechnol.* **5,** 1918–1923 (2006).

58. Saraogi, G. K., Gupta, P., Gupta, U. D., Jain, N. K. & Agrawal, G. P. Gelatin nanocarriers as potential vectors for effective management of tuberculosis. *Int. J. Pharm.* **385,** 143–149 (2010).

59. Zhao, Z., Li, Y. & Xie, M. Bin. Silk fibroin-based nanoparticles for drug delivery. *Int. J. Mol. Sci.* **16,** 4880–4903 (2015).

60. Mandal, B. B., Mann, J. K. & Kundu, S. C. Silk fibroin/gelatin multilayered films as a model system for controlled drug release. *Eur. J. Pharm. Sci.* **37,** 160–171 (2009).

61. Swaminathan, R., Ravi, V. K., Kumar, S., Kumar, M. V. S. & Chandra, N. *Lysozyme: A model protein for amyloid research*. *Advances in Protein Chemistry and Structural Biology* **84,** (2011).

62. Corradini, C. *et al.* Antimicrobial films containing lysozyme for active packaging obtained by sol-gel technique. *J. Food Eng.* **119,** 580–587 (2013).

63. Zhou, D., Yang, T., Qian, W., Xing, M. & Luo, G. Study of the mechanism of environmentally friendly translucent balsa-modified lysozyme dressing for facilitating wound healing. *Int. J. Nanomedicine* **13,** 4171–4187 (2018).

64. Decher, G. Fuzzy Nanoassemblies: Toward Layered Polymeric Multicomposites. *Science (80-.).* **277,** 1232–1237 (1997).

65. Caruso, F. Hollow Capsule Processing through Colloidal Templating and Self-Assembly. *Chem. - A Eur. J.* **6,** 413–419 (2000).

66. Estanqueiro, M., Amaral, M. H., Conceição, J. & Sousa Lobo, J. M. Nanotechnological carriers for cancer chemotherapy: The state of the art. *Colloids Surfaces B Biointerfaces* **126,** 631–648 (2015).

67. Cho, Y., Lee, J. B. & Hong, J. Controlled release of an anti-cancer drug from DNA structured nano-films. *Sci. Rep.* **4,** 4–8 (2014).

68. Jiang, B. & Li, B. Tunable drug loading and release from polypeptide multilayer nanofilms. *Int. J. Nanomedicine* **4,** 37–53 (2009).

69. Stana, J. *et al.* Multilayered Polysaccharide Nanofilms for Controlled Delivery of Pentoxifylline and Possible Treatment of Chronic Venous Ulceration. *Biomacromolecules* **18,** 2732–2746 (2017).

70. Riva, E. R. *et al.* PMMA/polysaccharides nanofilm loaded with adenosine deaminase inhibitor for targeted anti-inflammatory drug delivery. *Langmuir* **29,** 13190–13197 (2013).

71. Xie, M. *et al.* Non-covalent modification of graphene oxide nanocomposites with chitosan/dextran and its application in drug delivery. *RSC Adv.* **6,** 9328–9337 (2016).

72. Wang, L., Chen, D. & Sun, J. Layer-by-layer deposition of polymeric microgel films on surgical sutures for loading and release of ibuprofen. *Langmuir* **25,** 7990–7994 (2009).

73. Wang, L., Wang, X., Xu, M., Chen, D. & Sun, J. Layer-by-layer assembled microgel films with high loading capacity: Reversible loading and release of dyes and nanoparticles. *Langmuir* **24,** 1902–1909 (2008).

74. Hernández-Montelongo, J. *et al.* Nanofilms of hyaluronan/chitosan assembled layer-by-layer:

An antibacterial surface for Xylella fastidiosa. *Carbohydr. Polym.* **136,** 1–11 (2016).

75. Yucel, T., Lovett, M. L. & Kaplan, D. L. Silk-based biomaterials for sustained drug delivery. *J. Control. Release* **190,** 381–397 (2014).

76. Wang, X. *et al.* Nanolayer biomaterial coatings of silk fibroin for controlled release. *J. Control. Release* **121,** 190–199 (2007).

77. Hofmann, S. *et al.* Silk fibroin as an organic polymer for controlled drug delivery. *J. Control. Release* **111,** 219–227 (2006).

78. Mohanta, V., Madras, G. & Patil, S. Layer-by-Layer Assembled Thin Film of Albumin Nanoparticles for Delivery of Doxorubicin. *J. Phys. Chem. C* **116,** 5333–5341 (2012).

79. Donath, E., Sukhorukov, G. B., Caruso, F., Davis, S. A. & Möhwald, H. Novel Hollow Polymer Shells by Colloid-Templated Assembly of Polyelectrolytes. *Angew. Chemie Int. Ed.* **37,** 2201–2205 (1998).

80. Del Mercato, L. L. *et al.* Biological applications of LbL multilayer capsules: From drug delivery to sensing. *Adv. Colloid Interface Sci.* **207,** 139–154 (2014).

81. Cuomo, F., Lopez, F., Miguel, M. G. & Lindman, B. Vesicle-templated layer-by-layer assembly for the production of nanocapsules. *Langmuir* **26,** 10555–10560 (2010).

82. Du, P., Zhao, X., Zeng, J., Guo, J. & Liu, P. Layer-by-layer engineering fluorescent polyelectrolyte coated mesoporous silica nanoparticles as pH-sensitive nanocarriers for controlled release. *Appl. Surf. Sci.* **345,** 90–98 (2015).

83. Chen, Y., Lin, X., Park, H. & Greever, R. Study of artemisinin nanocapsules as anticancer drug delivery systems. *Nanomedicine Nanotechnology, Biol. Med.* **5,** 316–322 (2009).

84. Boudou, T. *et al.* Polyelectrolyte multilayer nanoshells with hydrophobic nanodomains for delivery of Paclitaxel. *J. Control. Release* **159,** 403–412 (2012).

85. Marchenko, I. *et al.* Controlled enzyme-catalyzed degradation of polymeric capsules templated on CaCO3: Influence of the number of LbL layers, conditions of degradation, and disassembly of multicompartments. *J. Control. Release* **162,** 599–605 (2012).

86. Szarpak, A. *et al.* Designing hyaluronic acid-based layer-by-layer capsules as a carrier for intracellular drug delivery. *Biomacromolecules* **11,** 713–720 (2010).

87. Itoh, Y., Matsusaki, M., Kida, T. & Akashi, M. Enzyme-responsive release of encapsulated proteins from biodegradable hollow capsules. *Biomacromolecules* **7,** 2715–2718 (2006).

88. Zhang, X., Lin, Y. & Gillies, R. J. Tumor pH and Its Measurement. *J. Nucl. Med.* **51,** 1167–1170 (2010).

89. Imoto, T., Kida, T., Matsusaki, M. & Akashi, M. Preparation and Unique pH-Responsive Properties of Novel Biodegradable Nanocapsules Composed of Poly(γ-glutamic acid) and Chitosan as Weak Polyelectrolytes. *Macromol. Biosci.* **10,** 271–277 (2010).

90. Cuomo, F. *et al.* pH-responsive liposome-templated polyelectrolyte nanocapsules. *Soft Matter* **8,** 4415 (2012).

91. Koo, H. Y., Lee, H.-J., Kim, J. K. & Choi, W. S. UV-triggered encapsulation and release from polyelectrolyte microcapsules decorated with photoacid generators. *J. Mater. Chem.* **20,** 3932–3937 (2010).

92. Tornaletti, S. & Pfeifer, G. P. UV damage and repair mechanisms in mammalian cells. *BioEssays* **18,** 221–228 (1996).

93. Javier, A. M. *et al.* Photoactivated release of cargo from the cavity of polyelectrolyte capsules

to the cytosol of cells. *Langmuir* **24,** 12517–12520 (2008).

94. Acharya, S., Dilnawaz, F. & Sahoo, S. K. Targeted epidermal growth factor receptor nanoparticle bioconjugates for breast cancer therapy. *Biomaterials* **30,** 5737–5750 (2009).

95. Pérez-Herrero, E. & Fernández-Medarde, A. Advanced targeted therapies in cancer: Drug nanocarriers, the future of chemotherapy. *Eur. J. Pharm. Biopharm.* **93,** 52–79 (2015).

96. Kamphuis, M. M. J. *et al.* Targeting of cancer cells using click-functionalized polymer capsules. *J. Am. Chem. Soc.* 1–5 (2010).

97. Cirstoiu-Hapca, A. *et al.* Nanomedicines for active targeting: Physico-chemical characterization of paclitaxel-loaded anti-HER2 immunonanoparticles and in vitro functional studies on target cells. *Eur. J. Pharm. Sci.* **38,** 230–237 (2009).

98. Choi, K. Y. *et al.* Self-assembled hyaluronic acid nanoparticles for active tumor targeting. *Biomaterials* **31,** 106–114 (2010).

99. Parveen, S. & Sahoo, S. K. Evaluation of cytotoxicity and mechanism of apoptosis of doxorubicin using folate-decorated chitosan nanoparticles for targeted delivery to retinoblastoma. *Cancer Nanotechnol.* **1,** 47–62 (2010).

100. Liang, C. *et al.* Improved therapeutic effect of folate-decorated PLGA-PEG nanoparticles for endometrial carcinoma. *Bioorganic Med. Chem.* **19,** 4057–4066 (2011).

101. Cucinotto, I. *et al.* Nanoparticle albumin bound Paclitaxel in the treatment of human cancer: nanodelivery reaches prime-time? *J. Drug Deliv.* **2013,** 905091 (2013).

102. Taheri, A. *et al.* Use of biotin targeted methotrexate-human serum albumin conjugated nanoparticles to enhance methotrexate antitumor efficacy. *Int. J. Nanomedicine* **6,** 1863–1874 (2011).

103. Gan, C. W. & Feng, S. S. Transferrin-conjugated nanoparticles of Poly(lactide)-d-α-Tocopheryl polyethylene glycol succinate diblock copolymer for targeted drug delivery across the blood-brain barrier. *Biomaterials* **31,** 7748–7757 (2010).

104. Epstein, J., Sanderson, I. R. & MacDonald, T. T. Curcumin as a therapeutic agent: The evidence from in vitro, animal and human studies. *Br. J. Nutr.* **103,** 1545–1557 (2010).

105. Xu, J., Fu, Y. & Chen, A. Activation of peroxisome proliferator-activated receptor-γ contributes to the inhibitory effects of curcumin on rat hepatic stellate cell growth. *Am. J. Physiol. Liver Physiol.* **285,** G20–G30 (2003).

106. Chen, A. & Xu, J. Activation of PPARγ by curcumin inhibits Moser cell growth and mediates suppression of gene expression of cyclin D1 and EGFR. *Am. J. Physiol. Liver Physiol.* **288,** G447–G456 (2005).

107. Reuter, S. *et al.* Effect of curcumin on nuclear factor κB signaling pathways in human chronic myelogenous K562 leukemia cells. *Ann. N. Y. Acad. Sci.* **1171,** 436–447 (2009).

108. Stöber, W., Fink, A. & Bohn, E. Controlled Growth of Monodisperse Silica Spheres in the Micron Size Range. *J. Colloid Interface Sci.* **26,** 62–69 (1968).

109. Pinto, R. J. B., Marques, P. A. A. P., Barros-Timmons, A. M., Trindade, T. & Neto, C. P. Novel SiO2/cellulose nanocomposites obtained by in situ synthesis and via polyelectrolytes assembly. *Compos. Sci. Technol.* **68,** 1088–1093 (2008).

110. Liu, Y. *et al.* Formation and characterization of natural polysaccharide hollow nanocapsules via template layer-by-layer self-assembly. *J. Colloid Interface Sci.* **379,** 130–140 (2012).

111. Kim, S. *et al.* PH- and glutathione-responsive release of curcumin from mesoporous silica nanoparticles coated using tannic acid-Fe(III) complex. *RSC Adv.* **5,** 90550–90558 (2015).

112. Taebnia, N. *et al.* Curcumin-Loaded Amine-Functionalized Mesoporous Silica Nanoparticles Inhibit α-Synuclein Fibrillation and Reduce Its Cytotoxicity-Associated Effects. *Langmuir* **32,** 13394–13402 (2016).

113. Silva, N. H. C. S., Pinto, R. J. B., Freire, C. S. R. & Marrucho, I. M. Production of lysozyme nanofibers using deep eutectic solvent aqueous solutions. *Colloids Surfaces B Biointerfaces* **147,** 36–44 (2016).

114. ISO 10993-5:2009 - Biological evaluation of medical devices -- Part 5: Tests for in vitro cytotoxicity. (2009).

115. Greasley, S. L. *et al.* Controlling particle size in the Stöber process and incorporation of calcium. *J. Colloid Interface Sci.* **469,** 213–223 (2016).

116. Ibrahim, I. A. M., Zikry, A. A. F. & Sharaf, M. A. Preparation of spherical silica nanoparticles: Stober silica. *J. Am. Sci.* **6,** 985–989 (2010).

117. Barisik, M., Atalay, S., Beskok, A. & Qian, S. Size dependent surface charge properties of silica nanoparticles. *J. Phys. Chem. C* **118,** 1836–1842 (2014).

118. Bagwe, R. P., Hilliard, L. R. & Tan, W. Surface modification of silica nanoparticles to reduce aggregation and nonspecific binding. *Langmuir* **22,** 4357–4362 (2006).

119. AbouAitah, K. *et al.* pH-controlled Release System for Curcumin based on Functionalized Dendritic Mesoporous Silica Nanoparticles. *J. Nanomed. Nanotechnol.* **07,** 1–11 (2016).

120. Nasab, N. A., Kumleh, H. H., Beygzadeh, M., Teimourian, S. & Kazemzad, M. Delivery of curcumin by a pH-responsive chitosan mesoporous silica nanoparticles for cancer treatment. *Artif. Cells, Nanomedicine Biotechnol.* **46,** 000 (2018).

121. Tiwari, N., Nawale, L., Sarkar, D. & Badiger, M. Carboxymethyl Cellulose-Grafted Mesoporous Silica Hybrid Nanogels for Enhanced Cellular Uptake and Release of Curcumin. *Gels* **3,** 8 (2017).

122. Schmid, F.-X. Biological Macromolecules: UV-visible Spectrophotometry. *Encycl. Life Sci.* 1–4 (2001). doi:10.1038/npg.els.0003142

123. Xue, C., Lin, T. Y., Chang, D. & Guo, Z. Thioflavin T as an amyloid dye: Fibril quantification, optimal concentration and effect on aggregation. *R. Soc. Open Sci.* **4,** (2017).

124. Umerska, A. *et al.* Polymeric Nanoparticles for Increasing Oral Bioavailability of Curcumin. *Antioxidants* **7,** 1–18 (2018).

125. Wang, M. *et al.* Curcumin induced HepG2 cell apoptosis-associated mitochondrial membrane potential and intracellular free Ca2+ concentration. *Eur. J. Pharmacol.* **650,** 41–47 (2011).

126. Syng-ai, C., Kumari, A. L. & Khar, A. Effect of curcumin on normal and tumor cells : Role of glutathione and bcl-2. *Mol. Cancer Ther.* **3,** 1101–1108 (2004).

127. Brkić Ahmed, L. *et al.* Impact of surface functionalization on the uptake mechanism and toxicity effects of silver nanoparticles in HepG2 cells. *Food Chem. Toxicol.* **107,** 349–361 (2017).

128. Ahmadian, E. *et al.* Effect of silver nanoparticles in the induction of apoptosis on human hepatocellular carcinoma (HepG2) cell line. *Mater. Sci. Eng. C* **93,** 465–471 (2018).

129. Li, Y. *et al.* Size-dependent cytotoxicity of amorphous silica nanoparticles in human hepatoma HepG2 cells. *Toxicol. Vitr.* **25,** 1343–1352 (2011).

130. Wittmaack, K. Novel dose metric for apparent cytotoxicity effects generated by in vitro cell exposure to silica nanoparticles. *Chem. Res. Toxicol.* **24,** 150–158 (2011).

131. Fröhlich, E. The role of surface charge in cellular uptake and cytotoxicity of medical nanoparticles. *Int. J. Nanomedicine* **7,** 5577–5591 (2012).

132. Riss, T. L. *et al. Cell Viability Assays*. *Assay Guidance Manual* (Eli Lilly & Company and the National Center for Advancing Translational Sciences, 2004).